frontiers | Frontiers in Marine Science

TYPE Original Research
PUBLISHED 23 October 2024
DOI 10.3389/fmars.2024.1454421

OPEN ACCESS

EDITED BY
Stelios Katsanevakis,
University of the Aegean, Greece

REVIEWED BY
Olga Mangoni,
University of Naples Federico II, Italy
Jun Sun,
China University of Geosciences, China

*CORRESPONDENCE
Karen J. Westwood
karen.westwood@aad.gov.au

†PRESENT ADDRESSES
Andreas Klocker,
NORCE Norwegian Research Centre,
Bjerknes Centre for Climate Research,
Bergen, Norway
Clara R. Vives,
Geobiology Department, Globe Institute,
University of Copenhagen, Copenhagen,
Denmark

‡These authors share first authorship

RECEIVED 25 June 2024
ACCEPTED 30 August 2024
PUBLISHED 23 October 2024

CITATION
Heidemann AC, Westwood KJ, Foppert A, Wright SW, Klocker A, Vives CR, Wotherspoon S and Bestley S (2024) Drivers of phytoplankton distribution, abundance and community composition off East Antarctica, from 55-80°E (CCAMLR Division 58.4.2 East). *Front. Mar. Sci.* 11:1454421. doi: 10.3389/fmars.2024.1454421

Drivers of phytoplankton distribution, abundance and community composition off East Antarctica, from 55-80°E (CCAMLR Division 58.4.2 East)

Asta C. Heidemann[1,2‡], Karen J. Westwood[1,3*‡], Annie Foppert[1,2], Simon W. Wright[2], Andreas Klocker[2†], Clara R. Vives[2,3†], Simon Wotherspoon[3] and Sophie Bestley[1,2]

[1]Australian Antarctic Program Partnership, University of Tasmania, Hobart, TAS, Australia, [2]Institute for Marine and Antarctic Studies, University of Tasmania, Hobart, TAS, Australia, [3]Australian Antarctic Division, Department of Climate Change, Energy, the Environment and Water, Kingston, TAS, Australia

Southern Ocean phytoplankton form the base of the Antarctic food web, influencing higher trophic levels through biomass and community structure. We examined phytoplankton distribution and abundance in the Indian Sector of the Southern Ocean during austral summer as part a multidisciplinary ecosystem survey: Trends in *Euphausiids* off Mawson, Predators and Oceanography (TEMPO, 2021). Sampling covered six meridional transects from 55-80°E, and from 62°S or 63°S to the ice edge. To determine phytoplankton groups, CHEMTAX analysis was undertaken on pigments measured using HPLC. Diatoms were the dominant component of phytoplankton communities, explaining 56% of variation in chlorophyll *a* (Chl *a*), with haptophytes also being a major component. Prior to sampling the sea ice had retreated in a south-westerly direction, leading to shorter ice-free periods in the west (< 44 days, ≤65° E) compared to east (> 44 days, ≥70°E), inducing a strong seasonal effect. The east was nutrient limited, indicated by low-iron forms of haptophytes, and higher silicate:nitrate drawdown ratios (5.1 east vs 4.3 west), pheophytin *a* (phaeo) concentrations (30.0 vs 18.4 mg m^{-2}) and phaeo:Chl *a* ratios (1.06 vs 0.53). Biological influences were evident at northern stations between 75-80°E, where krill "super-swarms" and feeding whales were observed. Here, diatoms were depleted from surface waters likely due to krill grazing, as indicated by high phaeo:Chl *a* ratios (> 0.75), and continued presence of haptophytes, associated with inefficient filtering or selective grazing by krill. Oceanographic influences included deeper mixed layers reducing diatom biomass, and a bloom to the north of the southern Antarctic Circumpolar Current Front in the western survey area thought to be sinking as waters flowed from west to east. Haptophytes were influenced by the Antarctic Slope Front with high-iron forms prevalent to the south only, showing limited iron transfer from coastal waters. Cryptophytes were associated with meltwater, and greens (chlorophytes + prasinophytes) were prevalent below the mixed layer. The interplay of seasonal, biological and oceanographic influences on phytoplankton populations during TEMPO had

parallels with processes observed in the BROKE and BROKE-West voyages conducted 25 and 15 years earlier, respectively. Our research consolidates understanding of the krill ecosystem to ensure sustainable management in East Antarctic waters.

KEYWORDS

pigment analysis, CHEMTAX, chlorophyll, phytoplankton composition, Southern Ocean, Antarctic ecosystem, krill-based foodwebs

1 Introduction

Primary production in Southern Ocean waters provides the basis for the Antarctic food web, directly influencing krill populations and consequently higher predators such as penguins, seals and whales (Nicol et al., 2010; Bestley et al., 2018, 2020; Krause et al., 2022; Lohmann et al., 2023). Potential shifts in phytoplankton biomass and community structure may therefore have important implications for the entire ecosystem (Deppeler and Davidson, 2017; Kim et al., 2018). In East Antarctica, the area between 55-80°E is known to be highly productive (Pinkerton et al., 2021). With a krill fishery developing in this region (Antarctic krill, *Euphausia superba*), ecological processes here need to be better understood to ensure sustainable ecosystem management.

The Southern Ocean is a High-Nutrient-Low-Chlorophyll (HNLC) zone where macronutrients such as nitrate and silicate are overabundant, but essential micro-nutrients, particularly iron, limit phytoplankton productivity (Boyd and Ellwood, 2010; Bazzani et al., 2023). Iron is supplied to the Southern Ocean through various mechanisms including sea-ice melt (Lannuzel et al., 2016), resuspended sediments from the Antarctic shelf (de Jong et al., 2013; Smith et al., 2021), and meltwater from ice shelves, glaciers and icebergs (Death et al., 2014; Duprat et al., 2016; Herraiz-Borreguero et al., 2016). Thus, chlorophyll *a* (Chl *a*) biomass is often higher near the coast of Antarctica compared to the open ocean (Westwood et al., 2010; Wright et al., 2010). The upwelling of Circumpolar Deep Water may also increase iron availability (Moreau et al., 2019; Smith et al., 2021), as well as remineralization of organic matter through microbial processes (Smetacek et al., 2004; Cavan et al., 2019). Light can also limit productivity in Southern Ocean waters (Vives et al., 2022), with mixed layer depths controlling the average irradiance received by cells in surface waters (Mitchell et al., 1991; Nelson and Smith, 1991). Phytoplankton biomass may also form distinct bands below the mixed layer in this region (Wright and van den Enden, 2000; Gomi et al., 2007; Westwood et al., 2010) with euphotic depth therefore being particularly important for these populations.

Whilst Chl *a* measurements provide a general indication of food stocks for krill, it is vital that phytoplankton community composition is also assessed given that size classes are known to change the efficiency of food webs (Trebilco et al., 2020). Research from the Western Antarctica Peninsula (WAP) has already shown that global warming can impact communities, with a shift from diatoms to smaller cryptophytes (Moline et al., 2004; Montes-Hugo et al., 2008; Mendes et al., 2023). Ocean acidification may also cause a shift to smaller cells, as demonstrated experimentally for East Antarctic waters (Davidson et al., 2016; Westwood et al., 2018). Large diatoms are known to form the main diet of krill, whereas smaller species such as cryptophytes, haptophytes and prasinophytes generally remain ungrazed (Meyer and El-Sayed, 1983; Kopczynska, 1992; Pauli et al., 2021). The persistence of small cells is thought to be either due to inefficient filtering by krill (Kawaguchi et al., 1999; Conroy et al., 2024) or selective feeding (Haberman et al., 2003), though feeding efficiency can increase if small cells are aggregated (Haberman et al., 2003; Liu et al., 2019). In contrast, salps and microzooplankton such as copepods and pteropods are highly efficient at grazing small cells (Deibel, 1985; Madin and Kremer, 1995; Pakhomov and Froneman, 2004; Venkataramana et al., 2019). However, this increases the complexity of the food web and is associated with less efficient energy transfer (Murphy et al., 2016).

Biogeochemical cycles may also be influenced by phytoplankton composition (Boyd et al., 2012; Murphy et al., 2021). The biological pump is influenced by cell size which affects the rate of carbon export as phytoplankton become senescent and sink (Smetacek, 1985; Acevedo-Trejos et al., 2015; Fan et al., 2020; Irion et al., 2021). In addition, selective vs generalized feeding by krill and zooplankton on various phytoplankton groups influences the re-packaging of cells into fecal material, which can be exported rapidly (Cavan et al., 2019; Trebilco et al., 2020). Climate may also be influenced by phytoplankton composition, with some species such as *Phaeocystis antarctica* (*P. antarctica*, haptophyte) being strong producers of dimethylsulfoniopropionate (DMSP, DiTullio and Smith, 1995). DMSP leads to the production of sulfate aerosols, promoting cloud formation and influencing earth's radiative budget (Jang et al., 2022).

Whilst comprehensive studies on phytoplankton composition and environmental drivers have been undertaken in the WAP and Ross Sea regions (Smith et al., 2014; Schofield et al., 2017; Bolinesi et al., 2020; van Leeuwe et al., 2020), less is known for East Antarctica. Similar to the Ross Sea, diatoms are known to be the dominant group, with haptophytes (mainly *P. antarctica*) also forming a major component (Davidson et al., 2010; Takao et al., 2014; Takahashi et al., 2022). However, there is high spatial and temporal variation for these and other taxa (Kawamura and Ichikawa, 1984; Gomi et al., 2005, 2007;

Davidson et al., 2010; Wright et al., 2010; Iida and Odate, 2014; Takahashi et al., 2022; Matsuno et al., 2023). The 1996 BROKE multidisciplinary voyage spanning 80°-150°E (Nicol et al., 2000) provided several insights into environmental drivers influencing phytoplankton in East Antarctica. They included grazing by krill or salps (Hosie et al., 2000; Wright and van den Enden, 2000), season (Waters et al., 2000), and influence from the Southern Boundary (SB) which when closer to the coast was associated with decreased sea ice extent and less production (Nicol et al., 2000). Blooms were found within melting pack ice but had variable phytoplankton composition, whereas cryptophytes and some dinoflagellates were prominent in grazed zones near the ice edge (Wright and van den Enden, 2000). Offshore, there were distinct sub-surface Chl *a* maxima with prasinophytes and haptophytes often prevalent within the temperature minimum (Tmin) layer (Wright and van den Enden, 2000). Diatoms were also associated with stratified conditions, whereas haptophytes were prevalent under mixed conditions (Wright and van den Enden, 2000). Overall, the drivers for different phytoplankton taxa were varied.

The 2006 BROKE-West multidisciplinary voyage (Nicol et al., 2010) conducted between 30°-80°E was an extension of BROKE and provided further insight into phytoplankton dynamics in East Antarctica (Davidson et al., 2010; Westwood et al., 2010; Wright et al., 2010). Based on detailed datasets from this voyage, and building on observations from BROKE, Wright et al. (2010) proposed a temporal sequence of phytoplankton composition as light starts to reach the water column during sea ice melt. They hypothesized that a primary bloom forms around 35 days before complete disappearance of sea ice, mainly composed of diatoms, haptophytes *(P. antarctica)*, and cryptophytes (Wright et al., 2010), seeded from the ice. The primary bloom becomes nutrient-limited and light-limited at depth due to self-shading, but the latter is relieved by krill grazing and increased light following ice melt. This allows a secondary bloom of (mainly) low-iron haptophytes to form at depth. Krill grazing at the retreating ice edge, combined with sedimentation of phytoplankton, causes iron to be exported to depth via sinking fecal pellets and detrital aggregations. This causes iron depletion in surface waters and removes opportunities for iron recycling in the upper water column. Offshore, where sea ice has been absent for longer periods and surface iron is depleted, a nanoflagellate community develops at depth consisting of haptophytes, dinoflagellates, prasinophytes (greens) and cryptophytes, as well as some small diatoms. The offshore population forms a distinct deep chlorophyll maximum (DCM) and represents a shade flora, positioned at a depth with just enough light for growth and sustained by recycled iron as well as residual and upwelled sources. To date, the temporal sequence proposed by Wright et al. (2010) has not been re-visited.

In 2021, the TEMPO voyage (Trends in *Euphausiids* off Mawson, Predators and Oceanography) was undertaken to gain a krill biomass estimate for East Antarctica and improve our understanding of the ecosystem to inform sustainable management practices for krill fishing (Kawaguchi et al. this issue). In this paper, our aim is to determine the patterns and drivers of phytoplankton distribution, abundance and community composition within the TEMPO survey area, since phytoplankton are the main food source for krill. The survey focused on the Commission for the Conservation of Antarctic Marine Living Resources (CCAMLR) management area 58.4.2 East (55-80°E) and provided the opportunity to expand on findings from the BROKE and BROKE-West surveys conducted 25 and 15 years earlier, respectively. Specifically, we aim to determine:

- Spatial patterns of phytoplankton biomass (Chl *a*) within the survey area.
- Patterns of phytoplankton community composition and how these are shaped through seasonal, biological and oceanographic influences, considering previous BROKE and BROKE-West observations.
- Potential parallels in the temporal sequence of phytoplankton composition hypothesized by Wright et al. (2010) for further validation.

2 Materials and methods

2.1 Survey and oceanography

The survey was undertaken during austral summer from 13th February to 12th March 2021 (Figure 1). Six north-south transects (T1 to T6) were conducted from west to east (55-80°E) with each extending from 62°S or 63°S to the sea ice edge. Three transects (60°E, 70°E, 80°E) coincided with the eastern transects of the BROKE-West voyage that was undertaken in 2006 (Nicol et al., 2010). An additional station (CTD 59) was undertaken between 75°E and 80°E to the north, where a krill "super-swarm" was detected. This aggregation was > 1 km and c. 100 m deep (M. Cox pers. comm.). There was also a significant number of whales (approx. 50, mostly humpback and some fin whales) and a krill super-swarm at the northern end of 80°E in the vicinity of CTD 60 (S. Kawaguchi pers. comm.), labelled as a "whale hot-spot" station.

CTD operations were conducted using Sea-Bird SBE911 instrumentation and 31 x 12 L Niskin bottles on a rosette. Additional sensors attached to the rosette included a photosynthetically active radiation (PAR) sensor and an ECO-Triplet for fluorescence measurements. To gain a high resolution of Chl *a* throughout the water column, high performance liquid chromatography (HPLC) Chl *a* data (see below) was regressed against fluorescence measurements from the same depths to provide calibrated fluorescence profiles.

Oceanographic fronts within the survey region are shown in Figure 1, as determined by Foppert et al. (2024). The Southern Antarctic Circumpolar Current Front (sACCF) and Southern Boundary (SB) were defined as the southernmost extents of the subsurface 1.8°C and 1.5°C isotherms, respectively (Williams et al., 2010; Bestley et al., 2020b). The Antarctic Slope Front (ASF) was defined to be where the subsurface 0°C isotherm deepened below 200 dbar from north to south, and was present along all transects but one (70°E, Figure 1). Lack of the ASF at 70°E may have been due to the presence of the Prydz Bay gyre which is known to extend offshore to approximately 65°S (Vaz and Lennon, 1996, Figure 1), or alternatively the ship did not travel far enough south to sample it due to heavy sea ice presence. Mixed layer depths were calculated

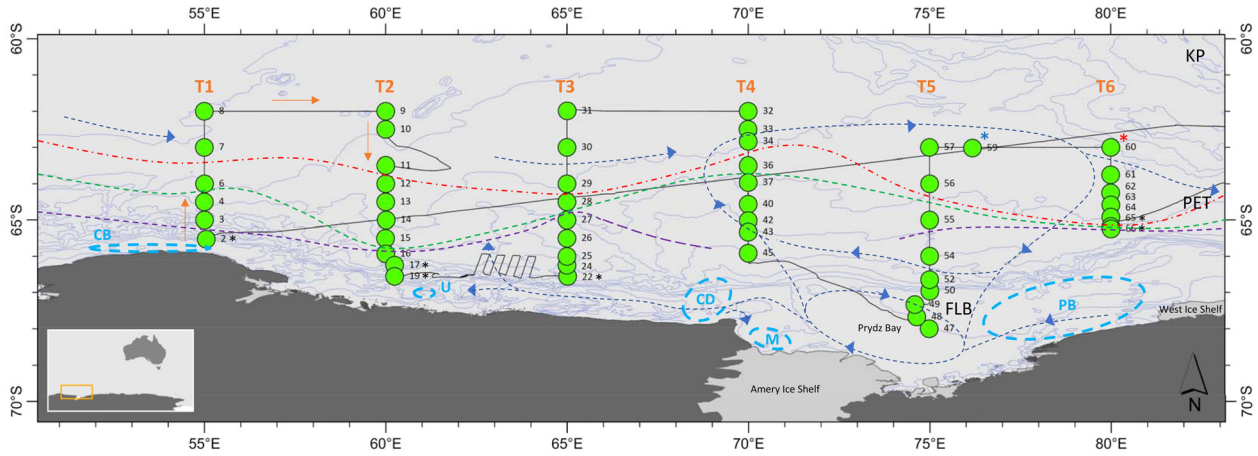

FIGURE 1
A schematic of the survey area showing CTD stations along Transects 1 - 6 (55-80°E), oceanographic fronts (after Foppert et al. (2024)), and 500 m depth contours. Red dashed line = sACCF, green dashed line = SB, purple dashed line = ASF. The approximate locations of gyres and currents are also indicated by blue dashed lines, after Smith and Trégure (1994), Vaz and Lennon (1996) and Williams et al. (2016). CTD station numbers are indicated and stations where ice was present are marked with a black asterisk. Sampling was undertaken from west to east. A krill super-swarm (defined as a dense aggregation > 1 km and c. 100 m deep) was located at CTD 59 – marked by a blue asterisk. A whale hot-spot (c. 50 whales) was located at CTD 60, with a krill super-swarm also present at this station – marked by a red asterisk. Locations of known polynyas are marked with light blue dashed circles; From west to east, CB = Cape Borle, U = Utstikkar Bay, CD = Cape Darnley, M = MacKenzie Bay, PB = Prydz Bay (consisting of Davis and Barrier polynyas combined), after Arrigo and van Dijken (2003) and Portela et al. (2021). The Kerguelen Plateau (KP), Princess Elizabeth Trough (PET), and Four Ladies Bank (FLB) are also indicated.

using a seawater density change of 0.03 kg m^{-3} from the near-surface (10 dbar, de Boyer Montégut et al., 2004, Foppert et al., 2024). The Tmin layer, where remnant winter water resides, was taken to be between the bottom of the mixed layer (as defined using the Δ 0.03 kg m^{-3} criterion) and the 0°C isotherm. For stations south of the ASF, Tmin was taken to be between the bottom of the mixed layer and 100 m. Euphotic depths were calculated as 1% incoming PAR, derived from vertical light extinction coefficients (K_d, Kirk, 1994).

Nutrients measured in Niskin bottle samples included silicate (Si), oxidized nitrogen (N), and ammonia, with sampling and analysis conducted according to standard procedures (Rees et al., 2019). As iron was not directly measured during the voyage, Si:N drawdown ratios were calculated as a proxy for iron limitation of phytoplankton, after Westwood et al. (2010), (see also Hutchins and Bruland, 1998). Briefly, average concentrations of Si and N in the mixed layer were subtracted from their respective average concentrations in the Tmin layer to determine nutrient drawdown by phytoplankton. Increased ratios are indicative of increased iron limitation.

2.2 Phytoplankton pigments

Pigments samples (1 L) were taken from Niskin bottles, filtered onto 13 mm GF/F filters in a darkened laboratory, then the filters placed in liquid nitrogen for later analysis. Six depths were sampled at each CTD station and always included the near-surface (5-10 m) and the depth of the DCM, as determined using real-time fluorescence data during downward CTD casts. In total 51 CTD stations were sampled. Pigments were later analyzed ashore using HPLC according to the method used in Wright et al. (2010). Briefly, filters were immersed in 300 µl 100% *N-N*-dimethylformamide and 50 µl methanol and incubated for 1 hour at -18°C. An internal standard (140 ng apo-8'-carotenal) was also added to improve analytical accuracy and to enable relative peak comparisons. Following incubation, the samples were mechanically disrupted using 0.7 mm zirconia beads in a mini-bead beater, then the extract was isolated from the filter/bead residue using centrifugation. The HPLC system used for analysis included a Gilson 233XL autosampler with 402 syringe pump, a Waters 1525 binary pump, a Symmetry C8 column maintained at 30°C by a water bath, a 2475 fluorescence detector and a 2998 photodiode array detector. For each HPLC run, 100 µl of sample was diluted with 25 µl water to improve peak quality (Jeffrey and Wright, 1997). Each sample injection was run for 40 minutes to allow sufficient time for solvent gradients to cycle through.

Pigments peaks were identified using Empower software (Waters) using known retention times determined through a standard mix (DHI) and a spectral absorption library (Zapata et al., 2000). Zeaxanthin and lutein peaks were difficult to distinguish due to interference from a smaller unknown peak that eluted at a similar time. These pigments were therefore analyzed under one peak named "ZeaLut". Chemotaxonomic analysis was undertaken using the software program CHEMTAX (Mackey et al., 1996; Wright et al., 1996). Nine phytoplankton taxa were initially chosen for analysis including chlorophytes, prasinophytes, cryptophytes, diatoms1, diatoms2, dinoflagellates1, dinoflagellates2, haptophytes8 high-iron, and haptophytes8 low-iron. This was based on previous experience within the survey region (Wright and van den Enden, 2000; Wright et al., 2010). Hierarchical clustering was undertaken on samples prior to analysis in CHEMTAX to reduce potential errors associated with

changes in pigment:Chl *a* ratios under varying environmental conditions such as light and nutrient availability (Wright et al., 2010). The R-Studio packages *cluster* and *dynamicTreeCut* were utilized, with the dynamic tree cutting method enabling detection of clusters dependent on their shape rather than the use of a fixed height cut-off (Langfelder et al., 2007; Hayward et al., 2023). The analysis resulted in 8 clusters sharing similar pigments.

To cross-check CHEMTAX outputs, light microscopy was undertaken on phytoplankton samples (1 L) that had been fixed in Lugol's iodine, taken at the same sites and depths as pigment samples. A total of 18 samples were examined, ensuring representation from each of the 8 clusters at the near-surface (5-10 m) and DCM, and from across each of the 6 transects. In some cases, it was clear that CHEMTAX was allocating a high proportion of Chl *a* to dinoflagellates2, whereas it should have been allocated to diatoms2. This was associated with the inclusion of gyroxanthin diester (gyrox) in the CHEMTAX analysis. There is evidence that gyrox may also be produced by haptophytes rather than solely dinoflagellates2 (Pettersen et al., 2011). Given high proportions of haptophytes in the samples it was decided to exclude gyrox and dinoflagellates2 from the CHEMTAX analysis and undertake a re-analysis. Chlorophytes and prasinophytes were also merged into "greens" for the re-analysis given the low biomass of these two groups. Table 1 shows revised phytoplankton groups and the initial pigment:Chl *a* ratios used for the second CHEMTAX run. Optimized ratios following the second run are also shown for Cluster 1, with values being within acceptable limits. As a further validation of CHEMTAX outputs, the pigment data was also analyzed using a new chemotaxonomic open-source R package *phytoclass* (Hayward et al., 2023) which uses a simulated annealing algorithm to derive phytoplankton groups. Results from the CHEMTAX and *phytoclass* analyses were strongly comparable with very little variance (Supplementary Figure 1).

Phaeophytin *a* (phaeo) pigment concentrations were also measured and utilized to gain insight into the growth stage of phytoplankton populations within the survey region. Phaeo is an oxidized degradation product of Chl *a* and thought to be a useful indicator of cell senescence (Gaffey et al., 2022), as well as grazing (Wright et al., 2010). The proportion of phaeo relative to Chl *a* can be used to indicate whether phytoplankton biomass reflects sampling during a growth phase, or during decline of the population. Comparisons of *in situ* samples with satellite-derived phenology have shown that phaeo:Chl *a* ratios < 28% suggest pre-peak growth, and higher values (> 0.28) a more senescent phase (Gaffey et al., 2022).

2.3 Ancillary data

Days since sea ice melt and distances to ice were determined from satellite. For sea ice calculations, daily passive microwave estimates of concentrations were obtained from the National Snow and Ice Data Centre SMMR-SSM/I polar product (Cavalieri et al., 1996; Maslanik and Stroeve, 1999), with ice cover <15% considered to be ice free. Data was obtained through the R package *raadtools* (Sumner, 2023). Maps of sea ice were produced using Nilas (Heil et al., 2023), showing daily 6 km concentrations using AMSR-E (Spreen et al., 2008, https://seaice.uni-bremen.de/sea-ice-

TABLE 1 (a) Initial pigment:Chl *a* ratios used in CHEMTAX, and (b) optimised ratios for Cluster 1 following analysis.

Class/Pigment	Chl c_3	Chl c_1	Peri	ButFuco	Fuco	19'-Hex	ZeaLut	Allo	Chl *b*	Chl *a*
(a) Initial										
Greens	0	0	0	0	0	0	0.012	0	0.31	1
Cryptophytes	0	0	0	0	0	0	0	0.36	0	1
Diatoms1	0	0.087	0	0	0.78	0	0	0	0	1
Diatoms2	0.065	0	0	0	1.02	0	0	0	0	1
Dinoflagellates1	0	0	0.54	0	0	0	0	0	0	1
Haptophytes8 high-iron	0.13	0	0	0.01	0.08	0.4	0	0	0	1
Haptophytes8 low-iron	0.27	0	0	0.12	0.02	1.1	0	0	0	1
(b) Optimised Cluster 1										
Greens	0	0	0	0	0	0	0.01	0	0.36	1
Cryptophytes	0	0	0	0	0	0	0	0.34	0	1
Diatoms1	0	0.07	0	0	0.68	0	0	0	0	1
Diatoms2	0.074	0	0	0	0.64	0	0	0	0	1
Dinoflagellates1	0	0	0.53	0	0	0	0	0	0	1
Haptophytes8 high-iron	0.05	0	0	0.01	0.08	0.51	0	0	0	1
Haptophytes8 low-iron	0.26	0	0	0.27	0.02	0.67	0	0	0	1

Pigment abbreviations are: Chl, chlorophyll; Peri, peridinin; ButFuco, 19'-butanoyloxyfucoxanthin; Fuco, fucoxanthin; 19'-Hex, 19'-hexanoyloxyfucoxanthin; Zea, zeaxanthin; Lut, lutein (ZeaLut pigment peaks combined); Allo, alloxanthin.

concentration/amsre-amsr2/). Maps of satellite-derived Chl *a* were produced via the ocean color climate change initiative (Sathyendranath et al., 2019) using merged products at 4 km resolution (OC-CCI ocean color data, Version 5, https://catalogue.ceda.ac.uk/uuid/1dbe7a109c0244aaad713e078fd3059a).

2.4 Models

Linear modelling, ANOVAs and General Additive Models (GAMs) were used to examine relationships between column-integrated phytoplankton and environmental variables. All modelling was undertaken in R (R Core Team, 2021). For linear modelling and ANOVAs, data was transformed where necessary based on box-cox and diagnostic plots. For 2-way ANOVAs, Tukey's HSD *post-hoc* tests were undertaken.

GAM analysis was undertaken using the R packages *mgcv* (Wood, 2017) and *visreg* (Breheny and Burchett, 2017). Parameters initially considered as predictors included mixed layer depth, days since ice melt, Tmin thickness, Tmin temperature, nitrogen concentrations in the Tmin layer and Si:N ratio. However, these needed to be reduced due to a high number of coefficients compared to a small sample size (n=51 stations). Following examination of separate GAMS for these parameters and the associated significance terms, a final GAM was fitted including mixed layer depth, days since sea ice melt, Si:N drawdown ratio (indicator of iron limitation) and nitrogen in the Tmin layer. Mixed layer depth and days since sea ice melt were found to be significant drivers of diatoms2 biomass (see below), so a similar GAM analysis was undertaken to also explore their effects on other phytoplankton taxa.

3 Results

3.1 Sea ice

Sea ice within the survey region retreated from north-east to south-west prior to the voyage commencing (Figures 2, 3). By mid-November the sea ice was already low to absent at the northern ends of 70-80°E. 55-65°E transects still had 100% ice cover along most of their length. The sea ice then retreated along the northern sections of 55-65°E throughout December. There was a gradual retreat south across all transects thereafter, with a minimum in February when voyage sampling commenced. By early to mid-March when sampling was being completed, the sea ice had started to re-form (Figure 2). As stations were undertaken from west to east, 55-65°E experienced more recent sea ice compared to other transects not only due to later melt, but also due to earlier sampling. 55-65°E and 80°E had sea ice present at southern-most stations at the time of sampling (Figure 3). The sea ice at the southern end of 80°E was newly formed. The southern stations on 70°E and 75°E did not have sea ice present at their sampling sites, though there was heavy sea ice in the surrounding area. Days since sea ice melt (defined as the number of days since a satellite pixel was 15% covered) ranged from 0-122 days at the time that samples were taken (Figure 3). The sACCF had a significant influence on the timing of sea ice melt with stations north of the sACCF melting earlier ($F_{1,49} = 45$, $p<0.001$, Figures 2, 3).

3.2 Chlorophyll distribution

Integrated Chl *a* concentrations (summed over 0-150 m) derived from high resolution fluorescence measurements ranged

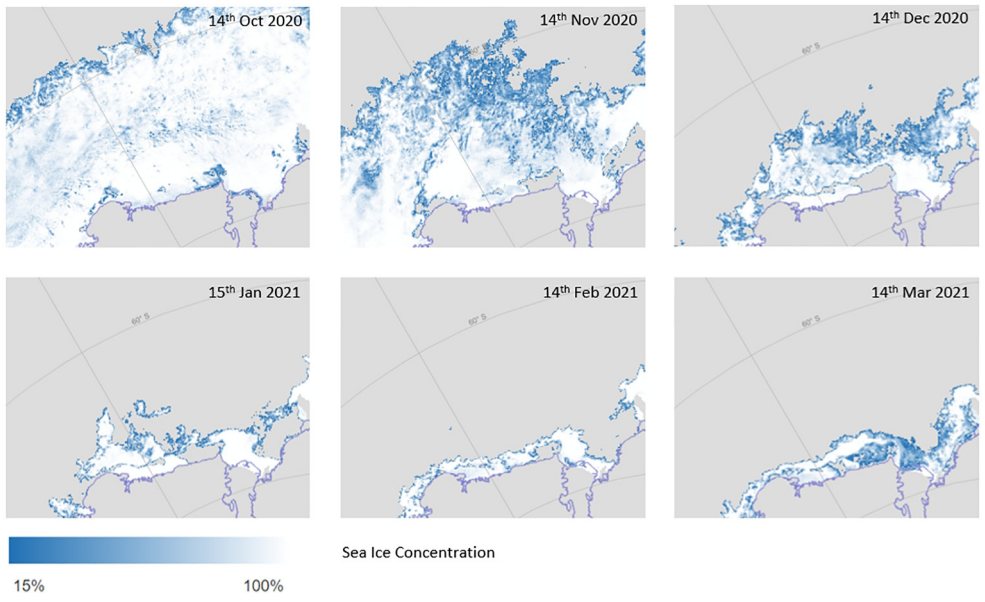

FIGURE 2
Sea ice concentrations (%) prior to and during the TEMPO voyage (Spreen et al., 2008).

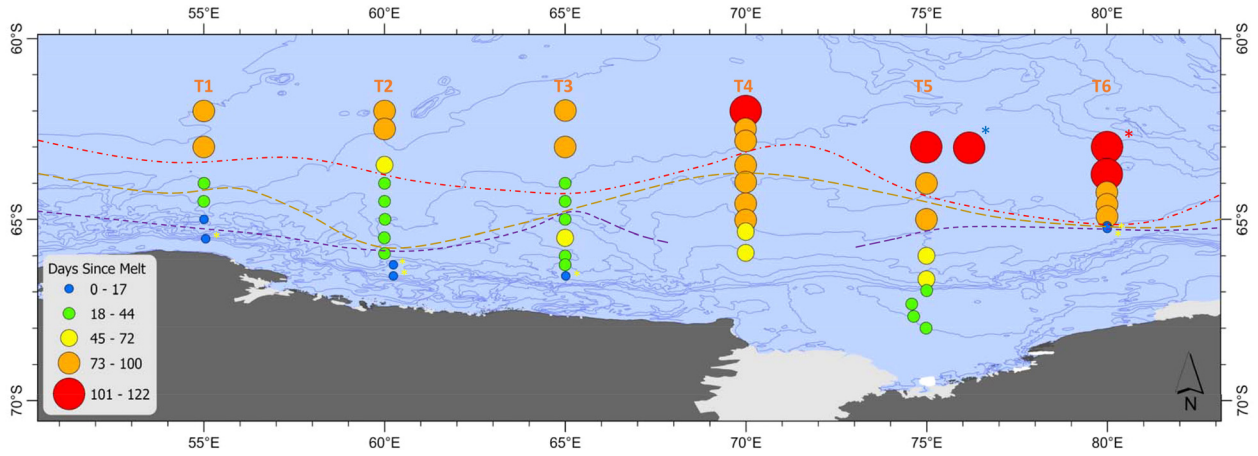

FIGURE 3
Days since sea ice melt at CTD stations along Transects 1-6 (55-80°E). Stations where sea ice was present are marked with a yellow asterisk. Red dashed line = sACCF, brown dashed line = SB, purple dashed line = ASF. The krill super-swarm station is marked by a blue asterisk. The whale hot-spot station is marked by a red asterisk.

from 18 to 102 mg m^{-2} (Figure 4). Chl *a* concentrations were elevated (> 61 mg m^{-2}) at the northern ends of 55°E and 60°E, the mid-section of 70°E, and the southern end of 80°E. At 75°E there were comparatively low Chl *a* concentrations (< 31 mg m^{-2}) on the shelf, but elevated concentrations at the continental slope and extending offshore. 65°E had relatively low Chl *a* along its length compared to the other transects. The krill super-swarm and whale hot-spot stations had notably low Chl *a* concentrations of < 24 mg m^{-2} (Figure 4).

Throughout the water-column Chl *a* concentrations ranged from 0.02 to 2.6 µg L^{-1}, with an average of 0.47 µg L^{-1} (Figure 5). Elevated Chl *a* concentrations at the northern end of 55°E were located within the mixed layer (Figure 5). In contrast, there was elevated Chl *a* below the mixed layer at 60°E and 65°E. The elevated Chl *a* stations across 55-65°E were all north of the sACCF (Figures 4, 5). South of the sACCF there were a number of Chl *a* "holes" (< 0.2 µg L^{-1}) within the mixed layer across 55-65°E (Figure 5). The well-defined nature of these holes, apparent at similar latitudes across transects, suggested that they may have been interlinked zonally, *i.e.* with the same hole spanning transects in association with currents.

The large offshore bloom along 75°E was located within the mixed layer (Figure 5) with Chl *a* concentrations as high as 2.6 µg L^{-1}. High Chl *a* along 70°E and 80°E were likely an east-west extension of this bloom. However, at 80°E most Chl *a* at the southern end was below the mixed layer rather than within it. This was due to shallow mixed layer depths associated with low salinity and temperature (Figure 5; Supplementary Figure 2), suggesting a meltwater lens at this location despite recent sea ice formation. 75°E showed an abrupt transition between the slope/offshore bloom and the shelf region, where comparatively low Chl *a* occurred throughout the water column (Figure 5). Elevated Chl *a* concentrations across 70-80°E

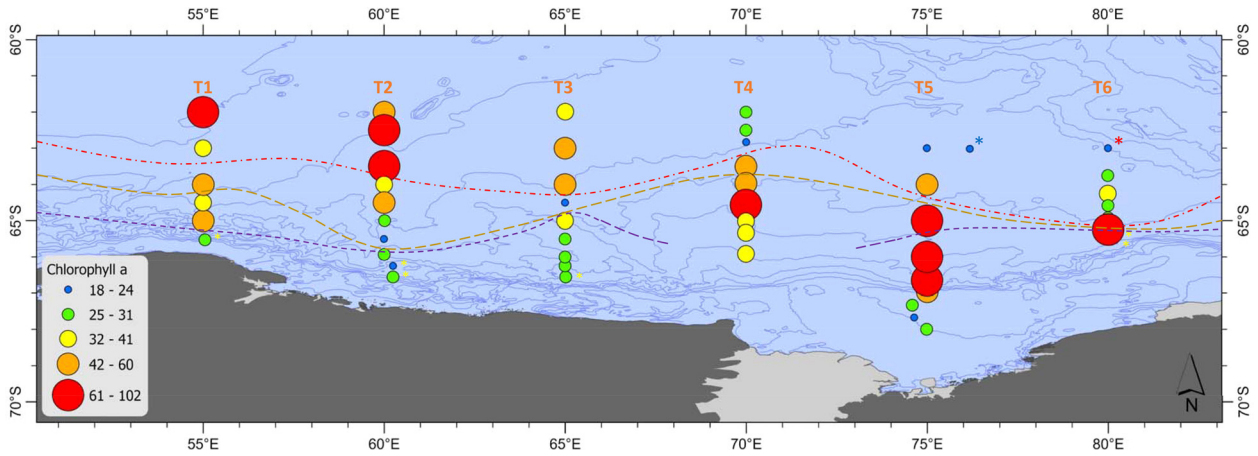

FIGURE 4
Integrated Chl *a* (10-150 m, mg m^{-2}) at stations along Transects 1 to 6 (55-80°E). Stations where sea ice was present are marked with a yellow asterisk. Red dashed line = sACCF, brown dashed line = SB, purple dashed line = ASF. The krill super-swarm station is marked by a blue asterisk. The whale hot-spot station is marked by a red asterisk.

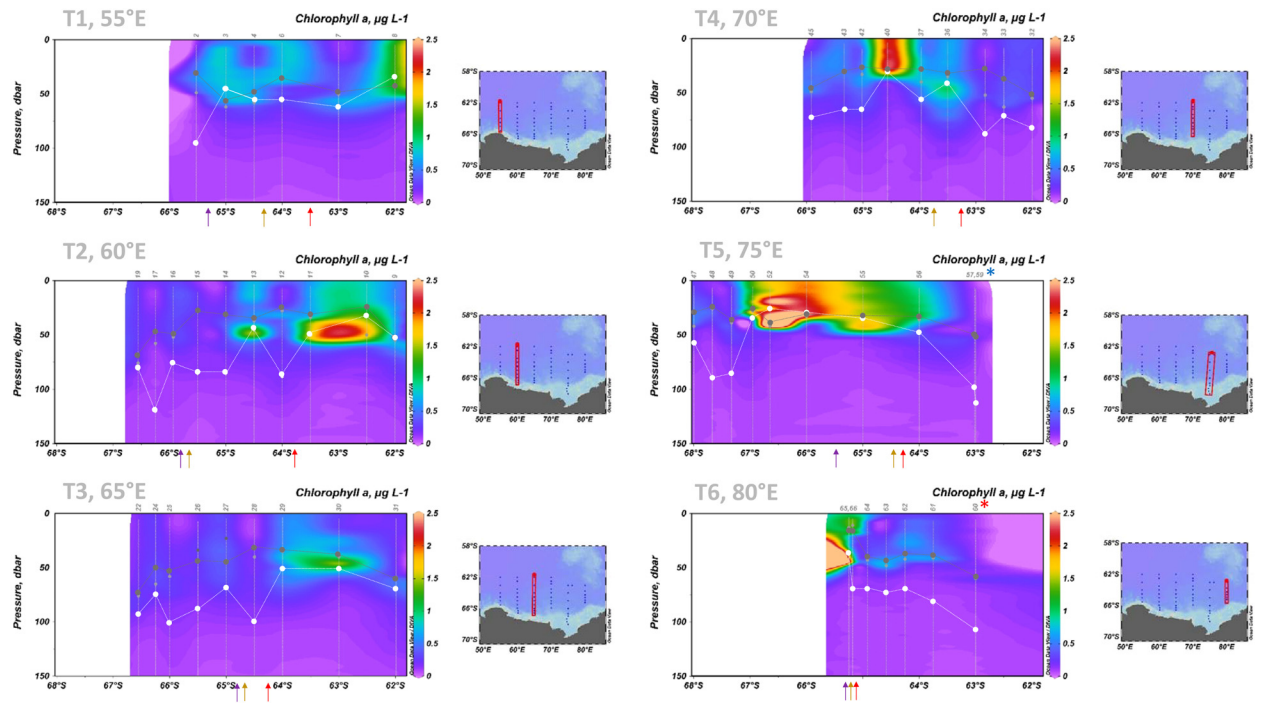

FIGURE 5
Chl *a* concentrations with depth (µg L^{-1}) along each transect (55-80°E). Dark grey circles with dashed lines are mixed layer depth calculated from density (kg m^{-3}), white circles with dashed lines are euphotic depth (m). Light grey circles are mixed layer depth calculated from maximum buoyancy frequency, for comparison with other studies. CTD station numbers are also shown. Data was interpolated between CTD stations using DIVA and plotted in Ocean Data View (Schlitzer, R., Ocean Data View, odv.awi.de, 2023). The krill super-swarm station is marked by a blue asterisk. The whale hot-spot station is marked by a red asterisk. Approximate frontal locations are indicated by arrows; red = sACCF, brown = SB, purple = ASF.

were all south of the SB (Figures 4, 5). North of the sACCF, there was low Chl *a* in surface waters at the krill super-swarm and whale hot-spot stations (Figures 4, 5).

Mixed layer depths ranged from 16 to 74 m (Figure 5), with shallowest depths at the southern end of 80°E due to the meltwater lens (see above). Euphotic depths ranged from 26-120 m (Figure 5), with depths of > 90 m at the krill super-swarm (75°E) and whale hot-spot (80°E) stations, as well as CTD 57 (in the vicinity of the krill super-swarm station) and CTDs 2, 17 and 25. These stations were all associated with low Chl *a*. At most stations, mixed layer depths were notably shallower than euphotic depths (Figure 5) so that cells circulating within the mixed layer would have experienced a high light environment. The exception was at stations where the 55-65°E and 70-80°E blooms occurred. At these locations, mixed depths were more similar to euphotic depths, and in some cases deeper, with circulating cells likely to experience periods of photo-limitation due to fluctuating light (Figure 5).

GAM analysis was used to further explore the major determinants of integrated Chl *a* stocks. The strongest association was a strong non-linear negative relationship with euphotic depth ($p < 0.001$, eff df= 3.23, R^2 adj=0.908, deviance explained=91.4%, Figure 6A). This clearly represented shading of the water column as biomass increased, rather than a negative response of phytoplankton to irradiance. There was also a non-linear relationship with days since sea ice melt ($p=0.014$, eff df = 3.46, R^2 adj=0.212, deviance explained=26.7%, n=51, Figure 6B). Biomass was high immediately following ice melt, slowly increased to a peak at 70 days, then declined. There were two high Chl *a* outliers evident (Figure 6B) – CTD 52 on the slope at 75°E, and CTD 66 at the southern end of 80°E. Both stations were associated with the 70-80°E bloom.

3.3 Satellite phenology

Ocean color data from satellites provided synoptic-scale patterns of Chl *a* in the lead up to, and during the voyage (Figure 7). The December composite showed there was elevated Chl *a* offshore (62-64°S) from 60-80°E in the vicinity of retreating sea ice. However, throughout February when sampling occurred this offshore Chl *a* was no longer visible. Similarly, the Prydz Bay polynya and West Ice Shelf were associated with consistently high Chl *a* on the shelf and offshore from December through to February (Figure 7), but by the time 70-80°E were sampled this visible surface Chl *a* had also decreased. Interestingly, there was a low Chl *a* band between the shelf and offshore in the Prydz Bay region during January and February, in the vicinity of the slope front (Figure 7). Ice cover hindered visibility in this region during March when *in situ* sampling was undertaken. The Cape Darnley and MacKenzie polynyas had peak Chl *a* concentrations in March, with the Cape Darnley autumn bloom achieving the highest surface concentrations evident within the survey area throughout the entire austral summer season. However, 70°E sampling in the vicinity of Cape Darnley was undertaken further offshore away from the polynya, and was also undertaken late February to early March so that these high Chl *a* concentrations

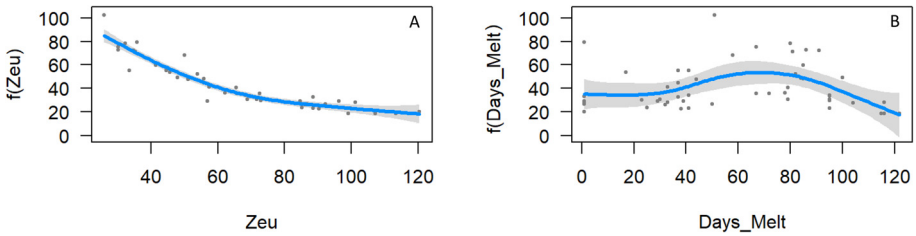

FIGURE 6
GAM analysis of integrated (10-150 m) Chl *a* showing the relationship with **(A)** euphotic depth, and **(B)** days since sea ice melt.

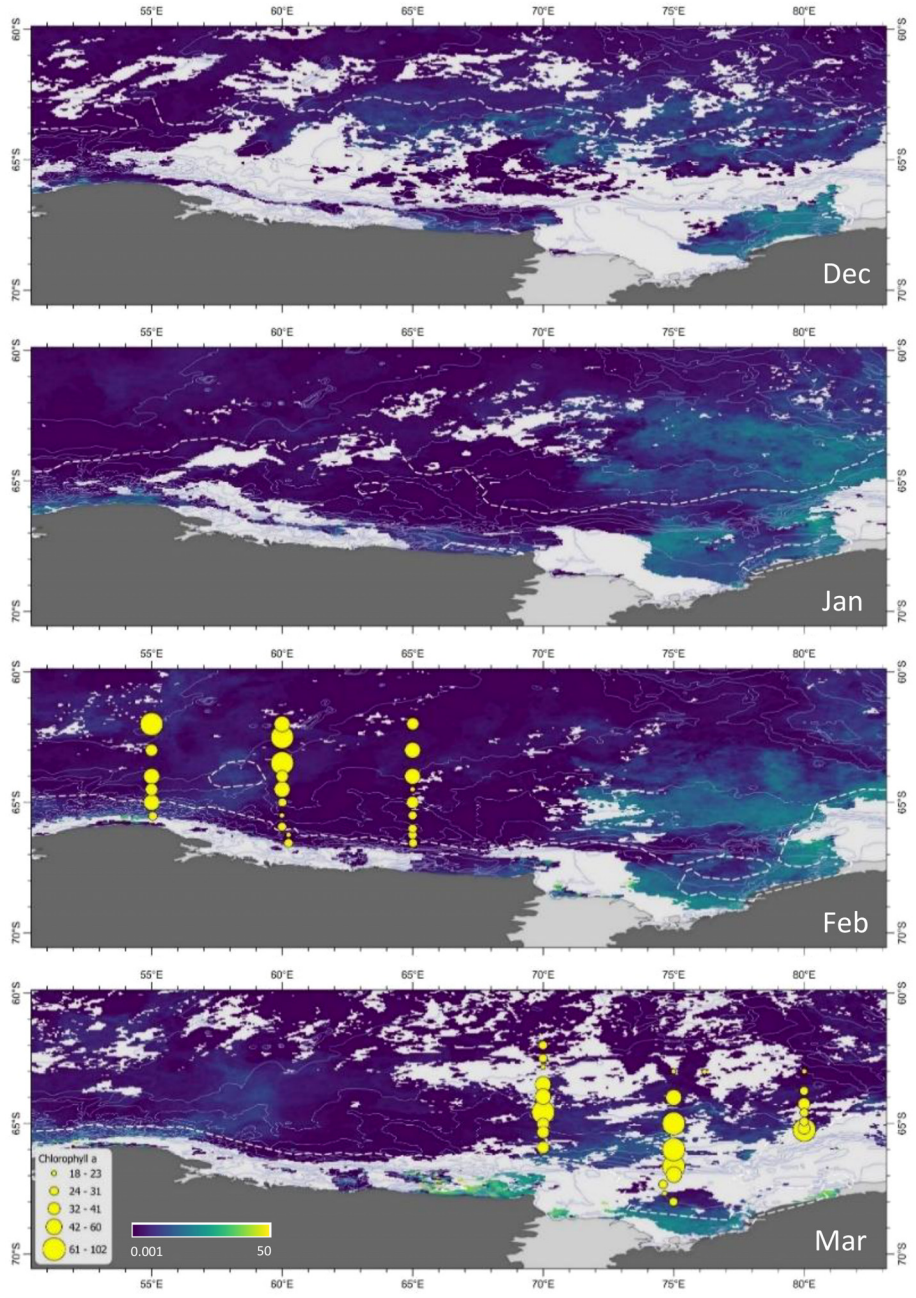

FIGURE 7
Chl *a* derived from monthly composites of ocean colour in the lead-up to and during the voyage (mg m^{-3}, Sathyendranath et al., 2019) and from HPLC pigment analysis during the voyage (mg m^{-2}, yellow circles). Depth contours (500 m) are shown as unbroken white lines. White dashed lines indicate 15% ice cover.

had likely not yet developed. Overall, *in situ* sampling of phytoplankton across the survey area appeared to occur post-peak of visible ocean color for most transects.

3.4 Phaeophytin and Si:N

Concentrations of phaeo ranged from 0 to 2.5 µg L^{-1} (Figure 8A). Measurements were significantly lower across 55-65° E (30.0 ± 16.4 mg m^{-2}) compared to 70-80°E (18.4 ± 12.5 mg m^{-2}, $F_{1,49}$ = 7.95, p=0.007), with a complete absence of phaeo at the southern end of 55°E. Concentrations did not noticeably change with depth for any given station. Phaeo:Chl *a* ratios showed that most phytoplankton populations in the survey area were in a decline phase, as indicated by proportions > 0.28 (Figure 8B). Cells in a growth phase (ratios < 0.28) were mainly in the western survey region across 55-65°E with these transects sampled earlier in the season (see above). Average ratios were significantly lower across 55-65°E (0.53 ± 0.3), compared to 70-80°E (1.06 ± 0.55, $F_{1,49}$ = 18.66, p< 0.005). Phaeo concentrations were not notably high at the krill super-swarm and whale hot-spot stations (Figure 8A), but this was likely associated with the very low biomass at these stations. In contrast, phaeo:Chl *a* ratios for these stations were high with values > 0.75 (Figure 8B).

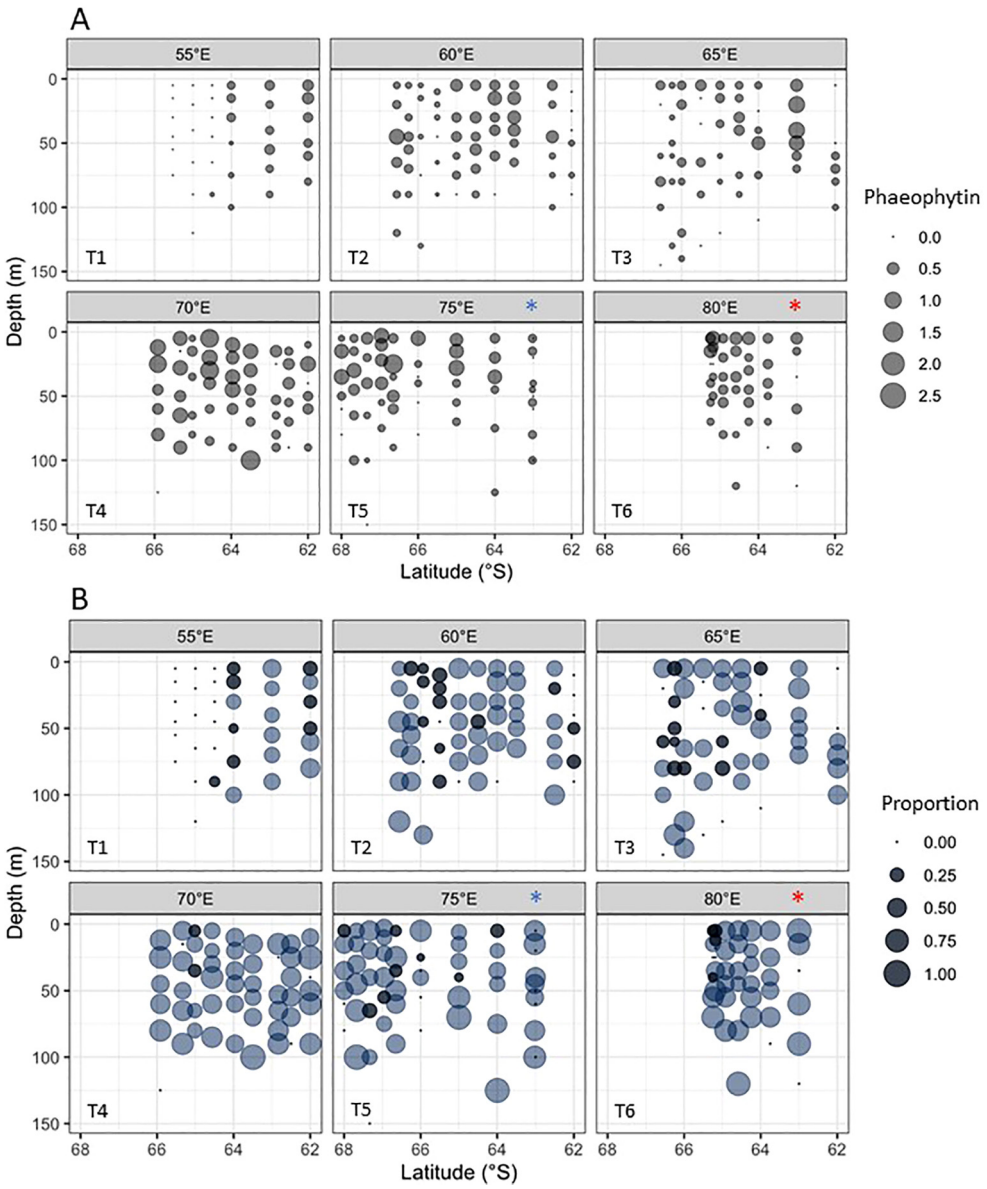

FIGURE 8
(A) Phaeophytin *a* (pheo) concentrations (µg L^{-1}), and **(B)** phaeo:Chl *a* ratios. Populations in a growth phase (ratios < 0.28) are indicated by dark blue circles. Light blue circles (ratios > 0.28) indicate populations in relative decline. Concentrations of 0 µg L^{-1} have been included to show locations where samples were taken. The krill super-swarm station is marked by a blue asterisk. The whale hot-spot station is marked by a red asterisk.

Macronutrient concentrations were generally non-limiting within the survey area, with nitrate ranging between 18.3-35.9 µM and silicate from 3.9-86.8 µM. The Si:N drawdown ratio was used as a proxy for iron limitation within the survey area (Hutchins and Bruland, 1998; Westwood et al., 2010), with higher ratios indicative of higher limitation. Si:N drawdown showed a similar pattern to phaeo:Chl *a* with ratios lower in the western survey area across 55-65°E (4.3 ± 0.7) compared to 70-80°E in the east (5.1 ± 0.7), with a one-way ANOVA showing that this difference was significant ($F_{1,49}$ = 8.9, p=0.004, Figure 9).

3.5 Phytoplankton community composition

Phytoplankton assemblages, determined using CHEMTAX analysis of pigments, had large spatial variations within the survey area (Figure 10). Diatoms2 was the most abundant group across all transects (Table 2), explaining 56% of variability in total Chl *a* with a strong linear relationship ($F_{1,49}$ = 65.5, R^2-adj= 0.56, p<0.001). Concentrations ranged from to 0.001 to 1.9 µg L^{-1}, with an average of 0.26 ± 0.34 µg L^{-1}. Microscopy showed that the pennate diatoms *Fragilariopsis* and *Pseudonitzschia* were the most represented genera within this group. The centric diatom *Thalassiosira* was also abundant as solitary cells. Haptophytes8 (high-iron and low-iron) were the second-most prevalent group, comprising almost 30% of total Chl *a*. There was variation as to which of the two iron groups dominated across the survey area, with a generally inverse relationship (Figure 10). Haptophytes8 high-iron were slightly more prevalent than low-iron overall, comprising 58% of the total haptophyte biomass. Concentrations of haptophytes8 high-iron ranged from 0 to 0.49 µg L^{-1}, with an average of 0.08 ± 0.08 µg L^{-1}. Haptophytes8 low-iron ranged from 0 to 0.45 µg L^{-1} with an average of 0.06 ± 0.06 µg L^{-1}. The primary species identified through light microscopy was *P. antarctica*, with both solitary cells and colonial forms present.

Diatoms1 were mainly found within the mixed layer across the survey region (Figure 10; Table 2). Concentrations ranged from 0 to 0.31 µg L^{-1} with an average of 0.016 ± 0.039 µg L^{-1}. In contrast, greens had highest biomass below the mixed layer (range 0 to 0.18 µg L^{-1}, average 0.02 ± 0.03 µg L^{-1}, Table 2) with their main prevalence at the southern ends of 65°E and 70°E, and off the shelf at 75°E. Similarly, dinoflagellates1 were more prevalent below the mixed layer, though biomass was relatively low (range 0 to 0.25 µg L^{-1}, average 0.014 ± 0.024 µg L^{-1}) and almost absent along 80°E. Cryptophytes were also low in biomass (range 0 to 0.14 µg L^{-1}, average 0.025 ± 0.017 µg L^{-1}) but were most prevalent at the southern-ends of 75°E (both on- and off-shelf) and 80°E. Cryptophyte populations were present both above and below the mixed layer (Figure 10; Table 2).

Elevated Chl *a* concentrations observed across the northern and mid-sections of 55-65°E (Figure 5) were associated with high abundances of diatoms2, north of the sACCF (Figure 10). The diatoms were clearly within the mixed layer at 55°E, but below the mixed layer at 60°E and 65°E. There were also elevated concentrations of haptophytes8 high-iron across 55-65°E, but cells were both above and below the mixed layer at 60°E and 65°E. Haptophytes8 high-iron were prevalent south of the ASF along most transects, particularly at 55°E, on the shelf at 75°E, and at 80°E (Figure 4). There were significantly lower densities of haptophytes8 high-iron north (6.3 ± 4.5 mg m^{-2}) compared to south of the ASF (9.5 ± 3.3 mg m^{-2}, $F_{1,49}$ = 6.11, p=0.017). Haptophytes low-iron were prevalent below the mixed layer across 55-65°E compared to surface waters (Figure 10; Table 2).

Elevated Chl *a* concentrations spanning 70-80°E south of the sACCF (Figure 5) were similarly associated with diatoms2 and haptophytes (Figure 10). However, in contrast to the bloom across 55-65°E, the haptophytes associated with the 70-80°E bloom in the eastern part of the survey area were predominantly low-iron rather than high-iron. Haptophytes low-iron were generally more prevalent in the eastern part of the survey area (70-80°E) compared to west (55-65°E).

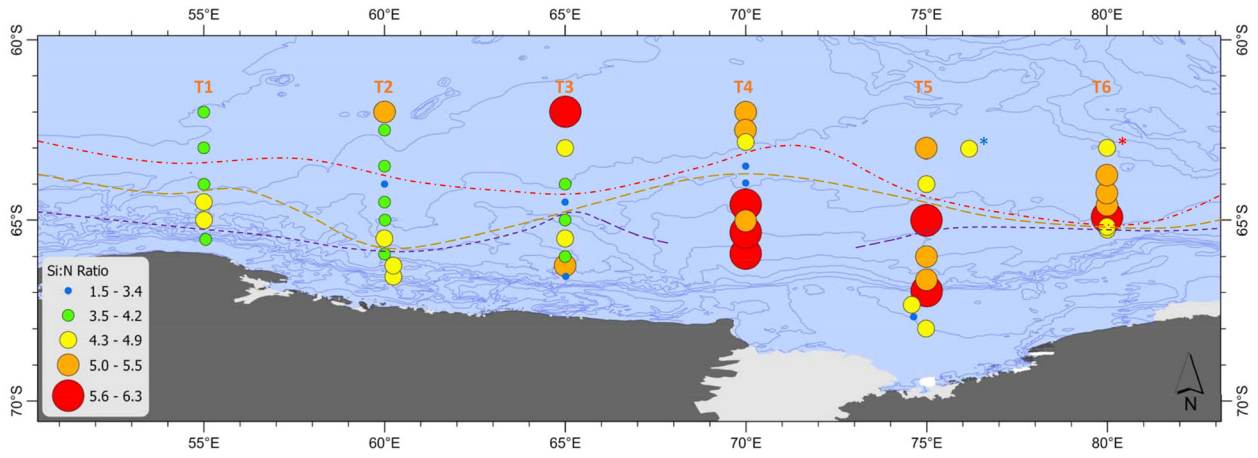

FIGURE 9
Silicate to nitrate ratios (Si:N) along Transects 1-6 (55-80°E). High ratios indicate high iron limitation and *vice versa*. Stations where sea ice was present are marked with a yellow asterisk. Red dashed line = sACCF, brown dashed line = SB, purple dashed line = ASF. The krill super-swarm station is marked by a blue asterisk. The whale hot-spot station is marked by a red asterisk.

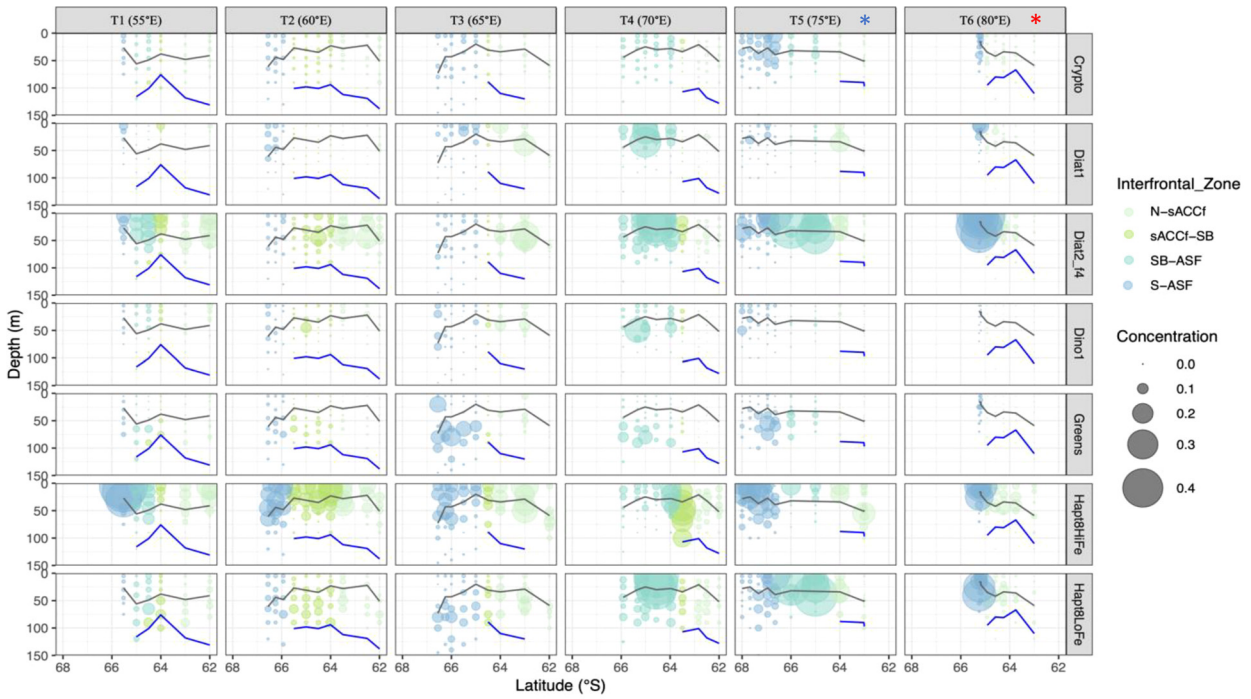

FIGURE 10
Depth profiles of phytoplankton taxa (μg L^{-1}) across the survey region. Mixed layer depths are shown as grey lines (Δ 0.03 kg m^{-3}), and the bottom of the Tmin layer shown as blue lines (note that deep values >150 m are not shown). Inter-frontal regions are coloured as per the key. Values of 0 μg L^{-1} have been included to show the locations where samples were taken. Due to high concentrations of diatoms2 they were reduced by a factor of 4 (f4) to improve visualisation. The krill super-swarm station is marked by a blue asterisk. The whale hot-spot station is marked by a red asterisk.

At the krill super-swarm station where there was low Chl *a* (see above), diatoms2 biomass was low throughout the water column (Figure 10). There was a high abundance of diatoms2 along 75°E, but an abrupt decrease in abundance where the krill were present. Similarly, at the whale hot-spot station there was low biomass of diatoms2 at the northern end of 80°E. Most other phytoplankton taxa were also absent at the krill super-swarm and whale hot-spot stations, except for haptophytes8 high iron.

3.6 Relationships with environmental variables

As diatoms2 were the dominant phytoplankton group and are the preferred food source for krill, the main modelling was undertaken on this taxon to further investigate relationships with environmental parameters. GAM analysis on column-integrated diatoms2 showed that mixed layer depth and days since sea ice melt were significant drivers of biomass (R^2-adj=0.36, deviance explained=46.9%, n=49, Figure 11). Diatoms2 biomass clearly decreased with deeper mixed layers (p=0.018, eff df=0.83). They also showed high biomass immediately following ice melt, a slight decrease, then similar to the Chl *a* model an increase between around 40 to 80 days post-melt, then a decline (p=0.022, eff df= 3.74). Nitrate concentration in the Tmin layer, Si:N drawdown and temperature of the Tmin layer had no significant influence on diatoms2.

For other phytoplankton taxa, mixed layer depth had a significant influence on two groups only; haptophytes8 low-iron (p=0.042, eff df=1.00, r2-adjusted=0.062, deviance explained=8.1%, Figure 12), and dinoflagellates1 (p=0.011, eff df=4.94, r2-adjusted=0.258, deviance explained=33.1%). However, the significant results were leveraged by the station with the deepest mixed layer (73 m at CTD 22). With this outlier removed the relationship for both taxa then became non-significant (p = 0.06 haptophytes8 low-iron, p=0.19 dinoflagellates1).

Days since ice melt influenced most phytoplankton groups, except dinoflagellates1 and diatoms1. Haptophytes8 high-iron decreased with days since melt (p=0.029, eff df=1.00, R^2-adjusted=0.075, deviance explained=9.4%, Figure 13), whereas haptophytes8 low-iron increased up until 70-80 days, then declined (p=0.036, eff df=2.69, R^2-adjusted=0.156, deviance explained=20.2%). Greens and cryptophytes remained relatively stable with days since ice melt, but started to decline at around 70 days post-melt (greens: p=0.003, eff df=2.34, R^2-adjusted=0.233, deviance explained=26.9%; cryptophytes: p=0.025, eff df=2.08, R^2-adjusted=0.150, deviance explained=18.5%). For all taxa, biomass declined at 95-120 days post-melt, with these stations all sampled 26th February or later, coinciding with the onset of austral autumn.

Overall, both mixed layer depth and days since ice melt had influences on phytoplankton populations within the survey region. One or both of these parameters influenced all taxa apart from dinoflagellates1 and diatoms1, noting that the influence of additional environmental parameters is not shown for taxa other

TABLE 2 Summary of key results for the seven major CHEMTAX phytoplankton groups.

Phytoplankton Group	Key Results
Cryptophytes	Low background concentrations across most of the survey area; Higher concentrations at southern stations on 75°E and 80°E; Biomass both above and below the mixed layer.
Diatoms1	Low background concentrations across most of the survey area; Most biomass within the mixed layer.
Diatoms2	The most abundant taxa comprising 56% of total Chl *a*; High abundances spanning 55-65°E north of the sACCF, and 70-80°E south of the sACCF and SB; Cells predominantly within the mixed layer at 55°E, 70°E and 75°E; Cells below the mixed layer at 60°E, 65°E and 80°E.
Dinoflagellates1	Low background concentrations across most of the survey area; Almost absent along 80°E; Highest concentrations found below the mixed layer at 70°E.
Greens	Prevalent below the mixed layer; High concentrations found at the southern ends of 65°E and 70°E, and off the shelf at 75°E.
Haptophytes8 high-iron	Prevalence south of the ASF along most transects; Associated with the 55-65°E bloom; Biomass both above and below the mixed layer; Cells still present at the krill super-swarm and whale hot-spot stations.
Haptophytes8 low-iron	Associated with the 70-80°E bloom; Biomass above and below the mixed layer across 70-80°E; Low concentrations in the western part of the survey area across 55-65°E, with cells prevalent in the Tmin layer.

than diatoms2. A preliminary analysis of additional parameters showed no meaningful patterns and were thus not pursued.

4 Discussion

The TEMPO survey off East Antarctica enabled the spatial distribution and temporal patterns of Chl *a* and phytoplankton communities to be described, as well as elucidating environmental drivers for these patterns. Variability was caused by an interplay of oceanographic, seasonal and biological influences that shaped populations. These are discussed further below. The survey also provided the opportunity to re-visit a similar region to the BROKE (Nicol et al., 2000) and BROKE-West (Nicol et al., 2010) voyages conducted 25 and 15 years earlier, respectively. The TEMPO survey differed from BROKE and BROKE-West in that it occurred about one month later and did not penetrate the sea ice zone. Nevertheless, the general patterns and features observed during TEMPO were similar to the previous voyages, and successional patterns relating to ice melt, krill grazing, and iron limitation were generally consistent with those described by Wright et al. (2010).

Chl *a* concentrations for TEMPO ranged from 0.02 to 2.6 μg L^{-1}, with an average of 0.47 μg L^{-1}, and integrated biomass from 18-102 mg m^{-2}. These concentrations were significantly lower than for BROKE-West (0.88-5.6 μg L^{-1}, average 1.2 μg L^{-1} and up to 328 mg m^{-2}, Wright et al., 2010), likely due to the ship being unable to enter sea ice where most productivity occurs (Strutton et al., 2000; Westwood et al., 2010). Maximum Chl *a* concentrations for BROKE (3.4 μg L^{-1}) were also higher than our study (Wright and van den Enden, 2000), though integrated concentrations were similar (27.4-103.0 mg m^{-2}). Diatoms2 was found to be the dominant taxon within the TEMPO survey region. This group therefore had a strong influence on Chl *a* distribution and explained 56% of variation. Haptophytes8 were the next dominant taxon and comprised 30% of Chl *a*. The dominance of diatoms and haptophytes was expected and agrees with other studies in the East Antarctic region (Davidson et al., 2010; Wright et al., 2010; Iida and Odate, 2014; Takao et al., 2014; Takahashi et al., 2022).

4.1 Oceanographic influences

There were two major blooms within the survey area, mainly consisting of diatoms2 and haptophytes8. The first bloom spanned 55-65°E north of the sACCF. Diatoms2 were within the mixed layer at 55°E, but below the mixed layer at 60°E and 65°E. Given the bloom was north of the sACCF this may suggest that the population was sinking as the current moved from west to east, with large and heavy cells observed such as *Fragilariopsis* and *Thalassiosira* having high export potential (Roca-Martí et al., 2017). Sinking may have been facilitated through nutrient limitation, though the northern sections of 55°E and 60°E were sampled closely in time. In contrast, haptophytes8 remained within the mixed layer across these transects, with the dominant species being motile cells of *P. antarctica*. The persistence of haptophytes8 in surface waters was therefore expected, given the small size of cells (< 5 μm) which

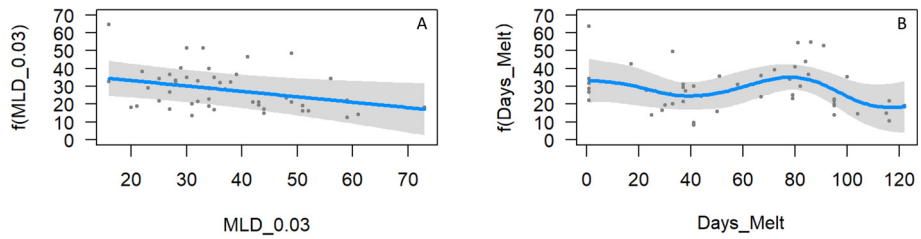

FIGURE 11
GAM analysis of diatoms2 showing the interactive relationship with **(A)** mixed layer depth, and **(B)** days since sea ice melt. Only parameters that had a significant influence are shown.

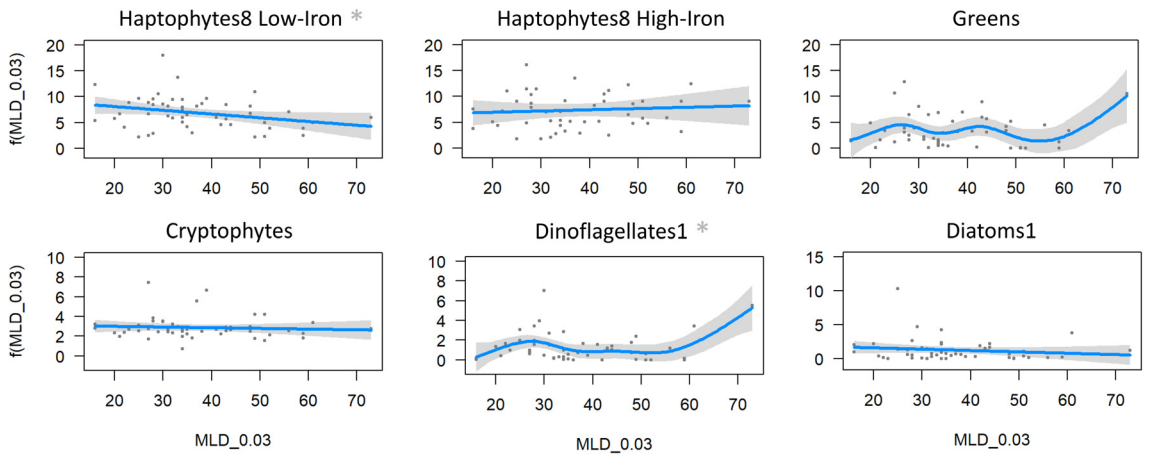

FIGURE 12
GAM analysis of the various phytoplankton taxa against mixed layer depth. Significant relationships are marked with an asterisk, but they are not significant when 73 m mixed layer depth is excluded.

hinders sinking, and evidence that the carbon flux of haptophytes is less efficient than for diatoms (Gowing et al., 2001; Wolf et al., 2016); although we note that rapid export of *P. antarctica* blooms can occur when cells are in colonial form (DiTullio et al., 2000). The second bloom spanned 70-80°E south of the SB. Again, this bloom was dominated by diatoms2 as well as haptophytes8, though in this case there was no evidence for the sinking of cells from surface waters. Satellite evidence suggested that the 70-80°E bloom was associated with advection from the Prydz Bay and West Ice Shelf regions. These regions may also be important for fueling blooms in the Princess Elizabeth Trough and Southern Kerguelen Plateau (Schallenberg et al., 2018). In the BROKE and BROKE-West surveys the SB was found to have an influence on production (Nicol et al., 2000; Wright et al., 2010). However, this was not found in our study given that blooms occurred both north and south of this front.

The main physical control on diatom2 populations was found to be mixed layer depth, with decreased biomass when mixed layer depth increased. Mixed layer depths were mostly shallower than euphotic depths throughout the survey area, so circulating cells did not experience photo-limitation. The preference of diatoms2 for shallower mixed layers and higher average irradiances agrees with the BROKE survey (Wright and van den Enden, 2000) and studies from other Antarctic regions including the Ross Sea (Arrigo et al., 1999), Western Antarctic Peninsula (Kopczynska, 1992; Schofield et al., 2017) and Northern Antarctic Peninsula (Costa et al., 2023). Diatoms are successful under stable light conditions due to low pigment concentrations per cell combined with high amounts of photoprotective pigment, allowing lower susceptibility to photoinhibition compared to other groups (Arrigo et al., 2010; Kropuenske et al., 2010). In fact, this group does not cope well with fluctuating light compared to other groups, due to slower photo acclimation processes (Larkum et al., 2003; Strzepek and Harrison, 2004; Kropuenske et al., 2010; van Leeuwe et al., 2020). Additional processes that may have contributed to decreased abundances included the entrainment of low Chl *a* water from depth (Smith

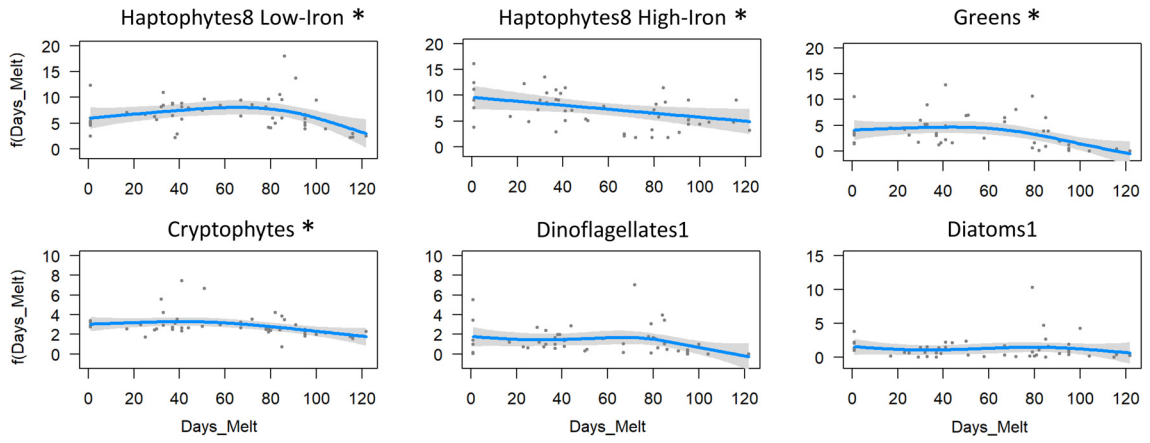

FIGURE 13
GAM analysis of the various phytoplankton taxa against days since ice melt. Significant relationships are marked with an asterisk.

et al., 2011), or increased particle aggregation from turbulence leading to export (Jones and Smith, 2017). Haptophytes were not affected by mixed layer depth in our study, but other studies have shown that they do favor mixed conditions (Wright and van den Enden, 2000). The main haptophyte, *P. antarctica*, is known to be highly adaptable to fluctuating light including under iron-limited conditions (Arrigo et al., 2010; van Leeuwe and Stefels, 2007; Kropuenske et al., 2010).

Haptophytes8 distribution was influenced by the ASF, in addition to seasonal influences described below. There were significantly higher concentrations of haptophytes8 high-iron south of the ASF across most transects, compared to north of the ASF. This pattern was very likely related to increased iron availability, with stations south of the ASF in closer vicinity to the Antarctic continental shelf and sea ice (Westwood et al., 2010). Shelf waters are known to supply sustained inputs of iron to surface waters through sediment resuspension (de Jong et al., 2013; Smith et al., 2021), with sea ice and melting from glaciers and ice shelves also being a significant source (Death et al., 2014; Duprat et al., 2016; Herraiz-Borreguero et al., 2016; Lannuzel et al., 2016). A significant change in haptophytes across the ASF confirms the physical influence of this front on nutrient availability, with reliance on cross-slope exchange processes such as frontal instabilities and eddies to influence transport (Heywood et al., 2014).

4.2 Seasonal effects

A second influence on haptophytes8 was season. North of the ASF there was a change in the relative proportion of high- and low-iron haptophytes8 from west to east across the survey area. Haptophytes8 high-iron were the prevalent form in the 55-65°E bloom and across the western survey region in general. In contrast, the 70-80°E bloom and general eastern survey region was dominated by low-iron forms, suggesting that this region was iron-limited. 55-65°E transects were sampled earlier in the season than 70-80°E. 55-65°E also experienced later sea ice melt, with retreat occurring across the survey area in a southwesterly direction. The combined influence of earlier sampling and later ice melt meant that most stations along 55-65°E were < 44 days post-melt. In contrast, the majority of 70-80°E stations were > 44 days post-melt (excepting stations on the shelf). Accordingly, GAM analysis showed that with increasing days since sea ice melt, haptophytes8 high-iron gradually decreased, whereas haptophytes8 low-iron increased, reflecting the differences observed between the western and eastern survey.

Pheophytin *a* (phaeo) concentrations and Si:N drawdown ratios further supported a strong seasonal influence on haptophytes8 and all other phytoplankton taxa within the survey area. Phaeo is a degradation product of Chl *a* (Jeffrey, 1997) and was significantly lower across 55-65°E compared to 70-80°E. It was also completely absent along sections of 55°E near the sea ice. Similarly, Si:N ratios were also significantly lower across 55-65°E suggesting less iron limitation of diatoms in this region (Hutchins and Bruland, 1998; Takeda, 1998; Franck et al., 2000). Finally, lower phaeo:Chl *a* ratios across 55-65°E compared to 70-80°E showed that 55-65°E populations to be in better health than 70-80°E populations. Interestingly however, most phaeo:Chl *a* ratios across the whole of the survey area were > 0.28 which suggested that cells were past their peak in growth at the time of sampling (Gaffey et al., 2022). This agreed with the satellite ocean color data which showed that by the time of sampling, Chl *a* that was previously present in surface waters had declined.

Despite clear changes in the health of phytoplankton between the western and eastern survey area, this was not reflected in column-integrated biomass for most taxa with days since sea ice melt only influencing the ratio of haptophytes high- and low- iron (see above) and diatoms2 over most of the growth season. This is discussed further in Section 4.5 below, in relation to the temporal sequence hypothesized by Wright et al. (2010). The main influence of days since sea ice melt was at the end of season with a decline in all taxa at > 95 days post-melt. These stations were all sampled 26th Feb or later, therefore coinciding with the onset of austral autumn. The last transect was completed on 12th March, by which time the sea ice had started to reform. Mixed layer depths for these final stations were not yet noticeably deeper. However, reduced daylength and lower angles of incoming light would have meant that cells were experiencing lower daily average irradiances, limiting productivity (Strutton et al., 2000). This would have allowed loss processes such as sinking and grazing to outweigh growth (Smith et al., 2000). Waters et al. (2000) also found decreased phytoplankton abundance with the onset of winter conditions during the BROKE survey.

4.3 Grazing

Large numbers of whales (c. 50) observed feeding at the northern end of 80°E (S. Kawaguchi pers. comm., April 2021), and krill super-swarms observed between 75°E and 80°E (M. Cox pers. comm., April 2021) indicated this region to be highly productive. Similarly, large numbers of humpback whales were previously observed feeding in the same vicinity in 2016 (A. Constable pers. comm. March 2016, K-Axis voyage, V3; 2015/16, RSV *Aurora Australis*), and tracking data has shown that Western Australian humpback whales visit this area from November to March (Bestley et al., 2019). Elevated climatological Chl *a* derived from satellite ocean color provides further evidence for high seasonal productivity here (Pinkerton et al., 2021). In addition, Foppert et al. (2024) found evidence of upwelling in this region during TEMPO, a process which likely increased nutrient availability for phytoplankton, and may support predictable foraging grounds for migrating baleen whales.

There was observational evidence for selective grazing of phytoplankton at the whale hot-spot and krill super-swarm stations located in this region. Diatoms2 had been stripped from surface waters, causing notably lower chlorophyll concentrations compared to the rest of the survey area. It is highly likely that diatoms2 had been grazed by krill, with their large cell size making them the preferred food source due to more efficient filtering (Meyer and El-Sayed, 1983). In contrast, small haptophytes remained within surface waters at both stations. This was likely

due either to inefficient filtering of small cells by krill (Kawaguchi et al., 1999; Conroy et al., 2024), or selective feeding on diatoms rather than haptophytes (Haberman et al., 2003). Phaeo: Chl *a* ratios at both stations were higher than elsewhere along these transects (> 0.75), also supporting the suggestion of heavy grazing. Interestingly, the haptophytes8 remaining in the water column at the whale hot-spot and krill super-swarm stations were high- rather than low-iron forms, despite these stations being offshore and in the eastern survey area. This suggests nutrient recycling, possibly through bacterial remineralization of krill or whale fecal material which is known to be iron rich (Ratnarajah et al., 2018). Sloppy feeding by krill may also have been a source of iron (Cavan et al., 2019).

A series of "holes" in surface Chl a (< 0.2 µg L-1) occurred across 55-65°E. Similar holes were also observed north of the ice edge during BROKE and BROKE West (Wright and van den Enden, 2000; Wright et al., 2010), which, during the latter cruise, closely matched the distribution of krill swarms grazing the ice-edge bloom. Comparison of Chl *a* and integrated krill biomass data in the vicinity of CTD stations during TEMPO showed no relationship across the survey area (data not shown). However, krill swarms are actively motile and the biomass measured at a specific time in the vicinity of a CTD station does not necessarily represent recent grazing pressure. Cox et al. (2022) found during the TEMPO voyage that small scale krill surveys can provide a good representation of the statistical distribution of krill densities across a larger scale, but only within the same latitudinal band. This potentially supports the hypothesis of the Chl *a* holes being interconnected across transects due to bands of high krill density. However, the Chl *a* holes were not strictly within the same latitudinal band, showing minor shifts to the south from 55°E to 65°E. Given these holes were present both north and south of the sACCF, SB and ASF it does not seem that fronts were influential.

4.4 Shelf waters

The only shelf stations within the survey area were at the southern end of 75°E in Prydz Bay. Here, there was an abrupt transition to low Chl *a* compared to the slope and offshore phytoplankton bloom (60-80°E). This transition may have been partly related to circulation patterns. The shelf stations (CTDs 47-50) were located across Four Ladies Bank which is known to act as a barrier to water exchange between the continental shelf and offshore (Smith and Trégure, 1994; Xu et al., 2019). There is a gyre within Prydz Bay associated with the outflow of supercooled ice shelf water from underneath the Amery Ice Shelf. This water is channeled offshore through the Amery Depression, with a weak return flow thought to exist across Four Ladies Bank to the Amery (Williams et al., 2016). It was therefore likely that the 75°E shelf stations were experiencing quite different oceanographic influences compared to offshore.

Krill grazing may also have been partly responsible for the abrupt transition to low Chl *a*, particularly given that diatoms2 was the main group depleted. Satellite observations showed high Chl *a* in this region from December through to February, but this had decreased by the time of sampling in early March. Within Prydz Bay the krill species *Euphausiia crystallorophias* would likely have been the dominant taxon responsible for grazing (Thomas and Green, 1988; Hosie and Cochran, 1994). Zooplankton other than krill also require consideration as grazers, with microzooplankton, copepods, pteropods and salps also prominent in Prydz Bay (Pearce et al., 2010; Hosie and Cochran, 1994; Li et al., 2001; Yang et al., 2013). These zooplankton groups efficiently ingest small phytoplankton cells (Johnston et al., 2021) however there was no clear evidence of this in the current study. Whilst there was a decrease in haptophytes8 low-iron on the shelf compared to the slope and offshore, there was a marked increase in haptophytes8 high-iron likely due to increased iron availability (see above), so the overall biomass of haptophytes8 remained essentially the same. Small cryptophytes were also present over the Prydz Bay shelf in higher concentrations than other transects. Regardless of whether circulation patterns and/or grazing influenced the transition in Chl *a* between the shelf and offshore, these regions have previously been shown to be ecologically distinct (Hosie and Cochran, 1994; Davidson et al., 2010).

4.5 Comparison with the BROKE-West temporal sequence

The patterns of phytoplankton biomass and composition during the TEMPO survey were consistent with those of BROKE-West and the latter part of the hypothesized temporal sequence proposed by Wright et al. (2010). Wright et al. (2010) proposed that a primary bloom forms around 35 days before complete disappearance of sea ice, which is seeded from the ice community, and consists mainly of diatoms2, high- and low-iron haptophytes8 and, to a lesser extent, cryptophytes. This bloom quickly exhausts iron stocks and is consumed by krill, allowing a secondary bloom of low-iron haptophytes at depth due to increased light there. The surface waters are left iron-depleted as iron has been exported to depth via the sinking of detrital aggregates from the primary bloom and krill fecal pellets following grazing. A nanoflagellate shade community then develops at depth utilizing recycled iron (Boyd and Ellwood, 2010) as well as residual or upwelled sources.

Several observations during TEMPO matched this sequence. First, our study showed highest biomass of diatoms2 and haptophytes8 immediately following ice melt, noting that we were unable to sample prior to melt. These populations were likely residual from a primary bloom that had developed under the ice. Takahashi et al. (2022) also recently showed evidence for the seeding of the water column by diatoms from sea ice communities. Second, the observed change from predominantly high-iron to low-iron haptophytes8 and patterns of Si:N drawdown are consistent with exhaustion of iron by the bloom (see above). Third, our study showed the development of a deep nanoflagellate community, consisting of greens and haptophytes. Greens were prevalent below the mixed layer across most transects, particularly across 65-75°E. Haptophyte8 low-iron were prevalent below the mixed layer across 55-65°E. The success of nanoflagellates at depth in low-iron environments is likely due to their small cell size, with

efficient uptake of recycled iron due to high surface area to volume ratios (Sunda and Huntsman, 1997; Li et al., 2009; Marañón, 2015).

However, there were also some differences from BROKE-West, which may be partly explained by TEMPO occurring a month later in the season. In the BROKE-West temporal sequence, diatoms2 decreased rapidly after 20 days post-melt, whereas in our study there was a slow decline from 0 to 40 days, implying that loss processes were slower. There was also a secondary increase in diatoms2 from 40-80 days post-melt in our study. This may simply have represented sites with few loss processes, with cells that had grown earlier in the season remaining in the water-column but slowly becoming senescent. Increased Si:N drawdown ratios and phaeo in our study supported this suggestion. Sexual reproduction may also have occurred leading to an increase in cell size, as recently shown by Matsuno et al. (2023) at 90-100 days post-melt.

Our study was also different from BROKE-West in that cryptophytes were not prevalent during TEMPO, with an average concentration of only 0.025 μg L^{-1}. In the Western Antarctic Peninsula where cryptophytes are prevalent (Hayward et al., 2024), high biomass is associated with low salinity (32.5-33.75 psu) and colder (-1 to 1°C) coastal waters (Schofield et al., 2017), with plumes extending as far as 100 km offshore (Moline et al., 2004). We identified a meltwater lens at southern stations on 80°E during the TEMPO voyage with salinity and temperature as low as 32.7 psu and -1.3°C at the surface, respectively (Foppert et al., 2024). Accordingly, cryptophyte abundances were higher in this region. There were also higher abundances of cryptophytes at the southern end of 75°E on the shelf in Prydz Bay and extending offshore. Whilst there was no clear meltwater lens at this location (Foppert et al., 2024), salinity and temperature were low in the southernmost surface waters sampled (CTD 47, 33.3 psu, -1.2°C), with both parameters gradually increasing to the north. A gradual increase in salinity and temperature along 75°E (rather than the abrupt changes seen at 80°E), may have been related to mixing associated with the gyre (see above, Williams et al., 2016).

Lastly, dinoflagellates1 were present in the deep nanoflagellate community during the BROKE-West survey (Wright et al., 2010) but this was not seen during TEMPO, apart from at one station at the southern end of 70°E where there were high concentrations within the Tmin layer. In general, abundances of dinoflagellates1 were lower for TEMPO than for BROKE-West. An almost complete absence of dinoflagellates1 along 80°E suggested that this taxon was strongly influenced by season, leading to the lower concentrations for the TEMPO survey.

4.6 Conclusions

The TEMPO survey represented the first large multidisciplinary survey off East Antarctica since the BROKE and BROKE-West surveys conducted 25 and 15 years earlier, respectively. It offered the opportunity to re-examine processes at the base of the food web in a region where krill fishing may expand, and to further understand the interplay of seasonal, biological and oceanographic drivers. Our data was broadly consistent with the previous surveys, and supported a temporal sequence in phytoplankton biomass and composition proposed for ice edge blooms.

The dominant phytoplankton groups were diatoms2 and haptophytes8, the latter with pigments that represented high- and low-iron forms. The primary drivers of biomass and composition included mixed layer depth, the ASF, seasonal changes, and iron depletion. There was also clear evidence of krill grazing, with a number of "holes" in the distribution of phytoplankton along transects. These holes appeared to mainly affect diatoms2 with clear depletion in surface waters. Haptophytes8 remained at these sites, suggesting selective grazing of the large diatoms by krill, or inefficient grazing of the smaller haptophyte cells. Greens and haptophytes low-iron were prevalent below the mixed layer and represented a nanoflagellate shade community similar to that observed for BROKE-West.

Whilst we found that phytoplankton populations and processes over the past 25 years were comparable across studies, the predicted loss of sea ice with climate change will likely influence phytoplankton composition into the future. The potential effects of such changes on krill populations and dependent organisms, as well as on carbon export, warrants further study on bloom development, particularly within the sea ice early in the season. Such data is vital as a base for ecosystem and carbon models. From a methodological standpoint, our study showed that a combination of pigment analysis for phytoplankton taxa (particularly the high- and low-iron forms of haptophytes8), phaeo:Chl *a* ratios, and Si:N drawdown ratios, provides valuable insights into the growth and grazing of phytoplankton and can be used to refine modelling efforts.

5 Additional requirements

All voyage activities were undertaken under an approved Notice of Determination and Authorization, in compliance with the Antarctic Treaty (Environment Protection Act) 1980. Phytoplankton/pigment samples were collected under AMLR Permit 20-23-4512 in compliance with the Marine Living Resources Conservation Act 1981.

Data availability statement

The datasets presented in this study can be found in online repositories. The names of the repository/repositories and accession number(s) can be found in the article/Supplementary Material.

Author contributions

AH: Formal analysis, Investigation, Visualization, Writing – original draft, Writing – review & editing. KW: Conceptualization, Data curation, Formal analysis, Funding acquisition, Investigation, Methodology, Project administration, Resources, Supervision, Visualization, Writing – original draft, Writing – review & editing. AF: Conceptualization, Formal analysis, Investigation, Supervision, Visualization, Writing – review & editing. SW: Formal analysis, Supervision, Writing – review & editing. AK:

Investigation, Writing – review & editing. CV: Investigation, Writing – review & editing. SW: Formal analysis, Writing – review & editing. SB: Conceptualization, Formal analysis, Investigation, Project administration, Supervision, Visualization, Writing – review & editing.

Funding

The author(s) declare financial support was received for the research, authorship, and/or publication of this article. This project was supported and funded by Australian Antarctic Science Projects 4512 and 4636, and received grant funding from the Australian Government as part of the Antarctic Science Collaboration Initiative program. This project also received financial support from Pew Charitable Trust and the Antarctic Science Foundation. We acknowledge the use of the CSIRO Marine National Facility (MNF, https://ror.org/01mae9353) in the form of sea-time on RV *Investigator*, and provision of support personnel, scientific equipment and data management. All data and samples from the voyage are publicly available as per MNF policy.

Acknowledgments

We would like to thank chief scientist Dr So Kawaguchi and deputy-chief scientist Mr Rob King for leading the voyage, and Ms Linda Gaskell (MNF) for voyage management. We also thank the captain and crew of RV *Investigator*, and MNF technical personnel for their support on the voyage. Thanks also to Dr Michael Sumner for ocean color maps, Dr Ben Raymond for sea ice data, and Dr Alexander Hayward for comparison of CHEMTAX and *phytoclass* outputs.

Conflict of interest

The authors declare that the research was conducted in the absence of any commercial or financial relationships that could be construed as a potential conflict of interest.

Publisher's note

Supplementary material

The Supplementary Material for this article can be found online at: https://www.frontiersin.org/articles/10.3389/fmars.2024.1454421/full#supplementary-material

References

Acevedo-Trejos, E., Brandt, G., Bruggeman, J., and Merico, A. (2015). Mechanisms shaping size structure and functional diversity of phytoplankton communities in the ocean. *Sci. Rep.* 5, 8918. doi: 10.1038/srep08918

Arrigo, K. R., Mills, M. M., Kropuenske, L. R., van Dijken, G. L., Alderkamp, A.-C., and Robinson, D. H. (2010). Photophysiology in two major Southern Ocean phytoplankton taxa: Photosynthesis and growth of *Phaeocystis Antarctica* and *Fragilariopsis cylindrus* under different irradiance levels. *Integr. Comp. Biol.* 50, 950–966. doi: 10.1093/icb/icq021

Arrigo, K. R., Robinson, D. H., Worthen, D. L., Dunbar, R. B., DiTullio, G. R., Vanwoert, M., et al. (1999). Phytoplankton community structure and the drawdown of nutrients and CO_2 in the Southern Ocean. *Science* 283, 365–367. doi: 10.1126/science.283.5400.365

Arrigo, K. R., and van Dijken, G. L. (2003). Phytoplankton dynamics within 37 Antarctic coastal polynya systems. *J. Geophys. Res. Oceans* 108, 3271. doi: 10.1029/2002JC001739

Bazzani, E., Lauritano, C., and Saggiomo, M. (2023). Southern Ocean iron limitation of primary production between past knowledge and future projections. *J. Mar. Sci. Eng.* 11, 272. doi: 10.3390/jmse11020272

Bestley, S., Andrews-Goff, V., van Wijk, E., Rintoul, S. R., Double, M. C., and How, J. (2019). New insights into prime Southern Ocean forage grounds for thriving Western Australian humpback whales. *Sci. Rep.* 9, 13988. doi: 10.1038/s41598-019-50497-2

Bestley, S., Raymond, B., Gales, N. J., Harcourt, R. G., Hindell, M. A., Jonsen, I. D., et al. (2018). Predicting krill swarm characteristics important for marine predators foraging off East Antarctica. *Ecography* 41, 996–1012. doi: 10.1111/ecog.03080

Bestley, S., Ropert-Coudert, Y., Bengtson Nash, S., Brooks, C. M., Cotté, C., Dewar, M., et al. (2020a). Marine ecosystem assessment for the southern ocean: birds and marine mammals in a changing climate. *Front. Ecol. Evol.* 8. doi: 10.3389/fevo.2020.566936

Bestley, S., van Wijk, E., Rosenberg, M., Eriksen, R., Corney, S., Tattersall, K., et al. (2020b). Ocean circulation and frontal structure near the southern Kerguelen Plateau: The physical context for the Kerguelen Axis ecosystem study. *Deep-Sea Res. II.* 174. doi: 10.1016/j.dsr2.2018.07.013

Bolinesi, F., Saggiomo, M., Ardini, F., Castagno, P., Cordone, A., Fusco, G., et al. (2020). Spatial-related community structure and dynamics in phytoplankton of the Ross Sea, Antarctica. *Front. Mar. Sci.* 7. doi: 10.3389/fmars.2020.574963

Boyd, P. W., Arrigo, K. R., Strzepek, R., and van Dijken, G. L. (2012). Mapping phytoplankton iron utilization: Insights into Southern Ocean supply mechanisms. *J. @ Geophys. Res. Oceans* 117, C06009. doi: 10.1029/2011JC007726

Boyd, P. W., and Ellwood, M. J. (2010). The biogeochemical cycle of iron in the ocean. *Nat. Geosci.* 3, 675–682. doi: 10.1038/ngeo964

Breheny, P., and Burchett, W. (2017). Visualization of regression models using *visreg*. *R. J.* 9, 56–71. doi: 10.32614/RJ-2017-046

Cavalieri, D. J., Parkinson, C. L., Gloersen, P., and Zwally, H. J. (1996). *Sea Ice Concentrations from Nimbus-7 SMMR and DMSP SSM/I-SSMIS Passive Microwave Data, Version 1* (NASA National Snow and Ice Data Center Distributed Active Archive Center).

Cavan, E. L., Belcher, A., Atkinson, A., Hill, S. L., Kawaguchi, S., McCormack, S., et al. (2019). The importance of Antarctic krill in biogeochemical cycles. *Nat. Commun.* 10, 4742. doi: 10.1038/s41467-019-12668-7

Conroy, J. A., Steinberg, D. K., Nardelli, S. C., and Schofield, O. (2024). Omnivorous summer feeding by juvenile Antarctic krill in coastal waters. *Limnol. Oceanogr.* 69, 874–887. doi: 10.1002/lno.12533

Costa, R. R., Ferreira, A., de Souza, M. S., Tavano, V. M., Kerr, R., Secchi, E. R., et al. (2023). Physical-biological drivers modulating phytoplankton seasonal succession along the Northern Antarctic Peninsula. *Environ. Res.* 231, 116273. doi: 10.1016/j.envres.2023.116273

Cox, M. J., Macaulay, G., Brasier, M. J., Burns, A., Johnson, O. J., King, R., et al. (2022). Two scales of distribution and biomass of Antarctic krill (Euphausia superba) in the eastern sector of the CCAMLR Division 58.4.2 (55°E to 80°E). *PloS One* 17, e0271078. doi: 10.1371/journal.pone.0271078

Davidson, A. T., McKinlay, J., Westwood, K., Thomson, P. G., van den Enden, R., de Salas, M., et al. (2016). Enhanced CO_2 concentrations change the structure of Antarctic marine microbial communities. *Mar. Ecol. Prog. Ser.* 552, 93–113. doi: 10.3354/meps11742

Davidson, A. T., Scott, F. J., Nash, G. V., Wright, S. W., and Raymond, B. (2010). Physical and biological control of protistan community composition, distribution and abundance in the seasonal ice zone of the Southern Ocean between 30 and 80°E. *Deep Sea Res. II* 57, 828–848. doi: 10.1016/j.dsr2.2009.02.011

Death, R., Wadham, J. L., Monteiro, F., Le Brocq, A. M., Tranter, M., Ridgwell, A., et al. (2014). Antarctic ice sheet fertilises the Southern Ocean. *Biogeosci.* 11, 2635–2643. doi: 10.5194/bg-11-2635-2014

de Boyer Montégut, C., Madec, G., Fischer, A. S., Lazar, A., and Iudicone, D. (2004). Mixed layer depth over the global ocean: An examination of profile data and a profile-based climatology. *J. Geophys. Res. Oceans* 109, C12003. doi: 10.1029/2004JC002378

Deibel, D. (1985). Clearance rates of the salp *Thalia democratica* fed naturally occurring particles. *Mar. Biol.* 86, 47–54. doi: 10.1007/BF00392578

de Jong, J., Schoemann, V., Maricq, N., Mattielli, N., Langhorne, P., Haskell, T., et al. (2013). Iron and land-fast sea ice of McMurdo Sound derived from sediment resuspension and wind-blown dust attributes to primary productivity in the Ross Sea, Antarctica. *Mar. Chem.* 157, 24–40. doi: 10.1016/j.marchem.2013.07.001

Deppeler, S. L., and Davidson, A. T. (2017). Southern Ocean phytoplankton in a changing climate. *Front. Mar. Sci.* 4. doi: 10.3389/fmars.2017.00040

DiTullio, G. R., Grebmeier, J. M., Arrigo, K. R., Lizotte, M. P., Robinson, D. H., Leventer, A., et al. (2000). Rapid and early export of *Phaeocystis Antarctica* blooms in the Ross Sea, Antarctica. *Nature* 404, 595–598. doi: 10.1038/35007061

DiTullio, G. R., and Smith, W. O. (1995). Relationship between dimethylsulfide and phytoplankton pigment concentrations in the Ross Sea, Antarctica. *Deep Sea Res. I Oceanogr. Res. Pap.* 52, 873–892. doi: 10.1016/0967-0637(95)00051-7

Duprat, L., Bigg, G., and Wilton, D. (2016). Enhanced Southern Ocean marine productivity due to fertilization by giant icebergs. *Nat. Geosci.* 9, 219–221. doi: 10.1038/ngeo2633

Fan, G., Han, Z., Ma, W., Chen, S., Chai, F., Mazloff, M. R., et al. (2020). Southern Ocean carbon export efficiency in relation to temperature and primary productivity. *Sci. Rep.* 10, 13494. doi: 10.1038/s41598-020-70417-z

Foppert, A., Bestley, S., Shadwick, E. H., Klocker, A., Vives, C. R., Liniger, G., et al (2024). Observed water-mass characteristics and circulation off Prydz Bay, East Antarctica. *Front. Mar. Sci.* 11, 1456207. doi: 10.3389/fmars.2024.1456207

Franck, V. M., Brzezinski, M. A., Coale, K. H., and Nelson, D. M. (2000). Iron and silicic acid concentrations regulate Si uptake north and south of the polar frontal zone in the Pacific Sector of the Southern Ocean. *Deep-Sea Res. II* 47, 3315–3338. doi: 10.1016/S0967-0645(00)00070-9

Gaffey, C. B., Frey, K. E., Cooper, L. W., and Grebmeier, J. M. (2022). Phytoplankton bloom stages estimated from chlorophyll pigment proportions suggest delayed summer production in low sea ice years in the northern Bering Sea. *PloS One* 17, e0267586. doi: 10.1371/journal.pone.0267586

Gomi, Y., Taniguchi, A., and Fukuchi, M. (2007). Temporal and spatial variation of the phytoplankton assemblage in the eastern Indian sector of the Southern Ocean in summer 2001/2002. *Polar Biol.* 30, 817–827. doi: 10.1007/s00300-006-0242-2

Gomi, Y., Umeda, H., Fukuchi, M., and Taniguchi, A. (2005). Diatom assemblages in the surface water of the Indian sector of the Antarctic surface water in summer of 1999/2000. *Polar Biosci.* 18, 1–15. doi: 10.15094/00006220

Gowing, M. M., Garrison, D. L., Kunze, H. B., and Winchell, C. J. (2001). Biological components of Ross Sea short-term particle fluxes in the austral summer of 1995–1996. *Deep-Sea Res. Part I: Oceanogr. Res. Papers* 48, 2645–2671. doi: 10.1016/S0967-0637(01)00034-6

Haberman, K. L., Ross, R. M., and Quetin, L. B. (2003). Diet of the Antarctic krill (*Euphausia superba* Dana): II. Selective grazing in mixed phytoplankton assemblages. *J. Exp. Mar. Biol. Ecol.* 283, 97–113. doi: 10.1016/S0022-0981(02)00467-7

Hayward, A., Pinkerton, M. H., and Gutiérrez-Rodriguez, A. (2023). *phytoclass*: A pigment-based chemotaxonomic method to determine the biomass of phytoplankton classes. *Limnol. Oceanogr. Methods* 21, 220–241. doi: 10.1002/lom3.10541

Hayward, A., Pinkerton, M. H., Wright, S. W., Gutiérrez-Rodriguez, A., and Law, C. S. (2024). Twenty-six years of phytoplankton pigments reveal a circumpolar Class Divide around the Southern Ocean. *Commun. Earth Environ.* 5, 92. doi: 10.1038/s43247-024-01261-6

Heil, P., Steketee, A., and Chua, S. (2023). Nilas Software - mapping tool for displaying multiple layers of physical and biogeochemical variables in the Southern Ocean. *Aust. Antarctic Data Centre*. doi: 10.26179/qh66-7p96

Herraiz-Borreguero, L., Lannuzel, D., van der Merwe, P., Treverrow, A., and Pedro, J. B. (2016). Large flux of iron from the Amery Ice Shelf marine ice to Prydz Bay. *J. Geophys. Res. Oceans* 121, 6009–6020. doi: 10.1002/2016JC011687

Heywood, K. J., Schmidtko, S., Hueze, C., Kaiser, J., Jickells, T. D., Queste, B. Y., et al. (2014). Ocean processes at the Antarctic continental slope. *Phil. Trans. R. Soc A* 372, 20130047. doi: 10.1098/rsta.2013.0047

Hosie, G. W., and Cochran, T. G. (1994). Mesoscale distribution patterns of macrozooplankton communities in Prydz Bay, Antarctica – January to February 1991. *Mar. Ecol. Prog. Ser.* 106, 21–39. Available at: http://www.jstor.org/stable/24844810.

Hosie, G. W., Schultz, M. B., Kitchener, J. A., Cochran, T. G., and Richards, K. (2000). Macrozooplankton community structure of East Antarctica (80-150°E) during the Austral summer of 1995/1996. *Deep-Sea Res. II* 47, 2437–2463. doi: 10.1016/S0967-0645(00)00031-X

Hutchins, D. A., and Bruland, K. W. (1998). Iron limited diatom growth and Si:N uptake ratios in a coastal upwelling regime. *Nature* 393, 561–564. doi: 10.1038/31203

Iida, T., and Odate, T. (2014). Seasonal variability of phytoplankton biomass and composition in the major water masses of the Indian Ocean sector of the Southern Ocean. *Polar Sci.* 8, 283–297. doi: 10.1016/j.polar.2014.03.003

Irion, S., Christaki, U., Berthelot, H., L'Helguen, S., and Jardillier, L. (2021). Small phytoplankton contribute greatly to CO_2-fixation after the diatom bloom in the Southern Ocean. *ISME J.* 15, 2509–2522. doi: 10.1038/s41396-021-00915-z

Jang, E., Park, K.-T., Yoon, Y. J., Kim, K., Gim, Y., Chung, H. Y., et al. (2022). First-year sea ice leads to an increase in dimethyl sulfide-induced particle formation in the Antarctic Peninsula. *Sci. Total Environ.* 803, 150002. doi: 10.1016/j.scitotenv.2021.150002

Jeffrey, S. W. (1997). "Application of pigment methods to oceanography," in *Phytoplankton Pigments in Oceanography: Guidelines to Modern Methods*. Eds. S. W. Jeffrey, R. F. C. Mantoura and S. W. Wright (UNESCO, Paris), 127–166, ISBN: .

Jeffrey, S. W., and Wright, S. W. (1997). "Qualitative and quantitative HPLC analysis of SCOR reference algal cultures," in *Phytoplankton Pigments in Oceanography: Guidelines to Modern Methods*. Eds. S. W. Jeffrey, R. F. C. Mantoura and S. W. Wright (UNESCO, Paris), 343–360, ISBN: .

Johnston, N. M., Murphy, E., Atkinson, A., Constable, A. J., Cotté, C., Cox, M., et al. (2021). Status, change and futures of zooplankton in the Southern Ocean. *Front. Ecol. Evol.* 17. doi: 10.3389/fevo.2021.624692

Jones, R. M., and Smith, W. O. (2017). The influence of short-term events on the hydrographic and biological structure of the southerwestern Ross Sea. *J. Mar. Syst.* 166, 184–195. doi: 10.1016/j.jmarsys.2016.09.006

Kawaguchi, S., Ichii, T., and Haganobu, M. (1999). Green krill, the indicator of micro- and nano-sized phytoplankton availability to krill. *Polar Biol.* 22, 133–136. doi: 10.1007/s003000050400

Kawamura, A., and Ichikawa, T. (1984). Distribution of diatoms in a small area in the Indian sector of the Antarctic. *Mem. Natn. Inst. Polar. Res. Spec. Issue* 32, 25–37.

Kim, H., Ducklow, H. W., Abele, D., Barlett, E. M. R., Buma, A. G. J., Meredith, M. P., et al. (2018). Inter-decadal variability of phytoplankton biomass along the coastal West Antarctic Peninsula. *Phil. Trans. R. Soc A* 376, 20170174. doi: 10.1098/rsta.2017.0174

Kirk, J. T. O. (1994). *Light and Photosynthesis in Aquatic Ecosystems. 2nd ed.* (Cambridge, United Kingdom: Cambridge University Press), ISBN: .

Kopczynska, E. E. (1992). Dominance of microflagellates over diatoms in the Antarctic areas of deep vertical mixing and krill concentrations. *J. Plankton Res.* 14, 1031–1054. doi: 10.1093/plankt/14.8.1031

Krause, D. J., Bonin, C. A., Goebel, M. E., Reiss, C. S., and Watters, G. M. (2022). The rapid population collapse of a key marine predator in the Northern Atlantic Peninsula endangers genetic diversity and resilience to climate change. *Front. Mar. Sci.* 8. doi: 10.3389/fmars.2021.796488

Kropuenske, L. R., Mills, M. M., van Dijken, G. L., Alderkamp, A.-C., Berg, G. M., Robinson, D. H., et al. (2010). Strategies and rates of photoacclimation in two major Southern Ocean phytoplankton taxa: *Phaeocystis Antarctica* (Haptophyta) and *Fragilariopsis cylindrus* (Bacillariophyceae). *J. Phycol.* 46, 1138–1151. doi: 10.1111/j.1529-8817.2010.00922.x

Langfelder, P., Zhang, B., and Horvath, S. (2007). Defining clusters from a hierarchical cluster tree: the Dynamic Tree Cut package for R. *Bioinformatics.* 24, 719–720. doi: 10.1093/bioinformatics/btm563

Lannuzel, D., Vancoppenolle, M., van den Merwe, P., de Jong, J., Meiners, K. M., Grotti., M., et al. (2016). Elementa. 4, 000130. doi: 10.12952/journal.elementa.000130

A. W. D. Larkum, S. E. Douglas and J. A. Raven (Eds.) (2003). *Photosynthesis in algae* (Dordrecht: Kluwer Academic Publishers), 480.

Li, W. K. W., McLaughlin, F. A., Lovejoy, C., and Carmack, E. C. (2009). Smallest algae thrive as the Arctic Ocean freshens. *Science* 326, 539. doi: 10.1126/science.1179798

Li, C., Sun, S., Zhang, G., and Ji, P. (2001). Summer feeding activities of zooplankton in Prydz Bay, Antarctica. *Polar Biol.* 24, 892–900. doi: 10.1007/s003000100292

Liu, M., Tao, Z., Zhang, Y., Yang, G., Sun, S., Li, C., et al. (2019). Feeding strategies of *Euphausia superba* in the eastern South Shetland Islands in austral summer. *Acta Oceanol. Sin.* 38, 75–83. doi: 10.1007/s13131-019-1392-8

Lohmann, A. C., Morton, J. P., Schofield, O. M., and Nowacek, D. P. (2023). Cyclical prey shortages for a marine polar predator driven by the interaction of climate change and natural climate variability. *Limnol. Oceanogr.* 68, 2668–2687. doi: 10.1002/lno.12453

Mackey, M. D., Mackey, D. J., Higgins, H. W., and Wright, S. W. (1996). CHEMTAX – a program for estimating class abundances from chemical markers: Application to HPLC measurements of phytoplankton pigments. *Mar. Ecol. Prog. Ser.* 144, 265–283. doi: 10.3354/meps144265

Madin, L., and Kremer, P. (1995). Determination of the filter-feeding rates of salps (Tunicata, Thaliacea). *ICES J. Mar. Sci.* 52, 583–595. doi: 10.1016/1054-3139(95)80073-5

Marañón, E. (2015). Cell size as a key determinant of phytoplankton metabolism and community structure. *Annu. Rev. Mar. Sci.* 7, 241–264. doi: 10.1146/annurev-marine-010814-015955

Maslanik, J., and Stroeve, J. (1999). *Near-Real-Time DMSP SSMIS Daily Polar Gridded Sea Ice Concentrations, Version 1* (NASA National Snow and Ice Data Center Distributed Active Archive Center).

Matsuno, K., Sumiya, K., Tozawa, M., Nomura, D., Sasaki, H., Yamaguchi, A., et al. (2023). Responses of diatom assemblages and life cycle to sea ice variation in the eastern Indian sector of the Southern Ocean during austral summer 2018/19. *Progr. Oceanogr.* 218, 103117. doi: 10.1016/j.pocean.2023.103117

Mendes, C. R. B., Costa, R. R., Ferreira, A., Jesus, B., Tavano, V. M., Dotto, T. S., et al. (2023). Cryptophytes: An emerging algal group in the rapidly changing Antarctic Peninsula marine environments. *Glob. Change Biol.* 29, 1791–1808. doi: 10.1111/gcb.16602

Meyer, M. A., and El-Sayed, S. (1983). Grazing of *Euphausia superba* Dana on natural phytoplankton populations. *Polar Biol.* 1, 193–197. doi: 10.1007/BF00443187

Mitchell, B. G., Brody, E. A., Holm-Hansen, O., McClain, C., and Bishop, J. (1991). Light limitation of phytoplankton biomass and macronutrient utilization in the Southern Ocean. *Limnol. Oceanogr.* 36, 1662–1677. doi: 10.4319/lo.1991.36.8.1662

Moline, M. A., Claustre, H., Frazer, T. K., Schofield, S., and Vernet, M. (2004). Alteration of the food web along the Antarctic Peninsula in response to a regional warming trend. *Glob. Change Biol.* 10, 1973–1980. doi: 10.1111/j.1365-2486.2004.00825.x

Montes-Hugo, M. A., Vernet, M., Martinson, D., Smith, R., and Iannuzzi, R. (2008). Variability on phytoplankton size structure in the western Antarctic Peninsula, (1997-2006). *Deep-Sea Res. Pt. II* 55, 2106–2117. doi: 10.1016/j.dsr2.2008.04.036

Moreau, S., Lannuzel, D., Janssens, J., Arroyo, M. C., Corkill, M., Cougnon, E., et al. (2019). Sea ice meltwater and circumpolar deep water drive contrasting productivity in three Antarctic polynyas. *JGR Oceans* 124, 2943–2968. doi: 10.1029/2019JC015071

Murphy, E. J., Cavanagh, R. D., Drinkwater, K. F., Grant, S. M., Heymans, J. J., Hofmann, E. E., et al. (2016). Understanding the structure and functioning of polar pelagic ecosystems to predict the impacts of change. *Proc. R. Soc B.* 283, 20161646. doi: 10.1098/rspb.2016.1646

Murphy, E. J., Johnston, N. M., Hofmann, E. E., Phillips, R. A., Jackson, J. A., Constable, A. J., et al. (2021). Global connectivity of Southern Ocean ecosystems. *Front. Ecol. Evol.* 9. doi: 10.3389/fevo.2021.624451

Nelson, D. M., and Smith, J. W. O. (1991). Sverdrup revisited: critical depths, maximum chlorophyll levels, and the control of Southern Ocean productivity by the irradiance-mixing regime. *Limnol. Oceanogr.* 36, 1650–1661. doi: 10.4319/lo.1991.36.8.1650

Nicol, S., Pauly, T., Bindoff, N. L., and Strutton, P. G. (2000). BROKE, a biological/oceanographic survey off the coast of East Antarctica (80-150°E) carried out in January-March 1996. *Deep Sea Res. II* 47, 2281–2298. doi: 10.1016/S0967-0645(00)00026-6

Nicol, S., Raymond, B., and Meiners, K. (2010). BROKE-West, a large ecosystem survey of the South West Indian Ocean sector of the Southern Ocean, 30°E-80°E (CCAMLR Division 58.4.2). *Deep-Sea Res. II.* 57, 693–700. doi: 10.1016/j.dsr2.2009.11.002

Pakhomov, E., and Froneman, P. (2004). Zooplankton dynamics in the eastern Atlantic sector of the Southern Ocean during the austral summer 1997/1998 - Part 2: Grazing impact. *Deep-Sea Res. Pt. II* 51, 2617–2631. doi: 10.1016/j.dsr2.2000.11.002

Pauli, N.-C., Metfies, K., Pakhomov, E. A., Neuhaus, S., Graeve, M., Wenta, P., et al. (2021). Selective feeding in Southern Ocean key grazers—diet composition of krill and salps. *Commun. Biol.* 4, 1061. doi: 10.1038/s42003-021-02581-5

Pearce, I., Davidson, A. T., Thomson, P. G., Wright, S., and van den Enden, R. (2010). Marine microbial ecology off East Antarctica (30-80°E): Rates of bacterial and phytoplankton growth and grazing by heterotrophic protists. *Deep-Sea Res.* 57, 849–862. doi: 10.1016/j.dsr2.2008.04.039

Pettersen, R., Johnsen, G., Berge, J., and Hovland, E. K. (2011). Phytoplankton chemotaxonomy in waters around the Svalbard archipelago reveals high amounts of Chl *b* and presence of gyroxanthin-diester. *Polar Biol.* 34, 627–635. doi: 10.1007/s00300-010-0917-6

Pinkerton, M. H., Boyd, P. W., Deppeler, S., Hayward, A., Höfer, J., and Moreau, S. (2021). Evidence for the impact of climate change on primary producers in the southern ocean. *Front. Ecol. Evol.* 9. doi: 10.3389/fevo.2021.592027

Portela, E., Rintoul, S. R., Bestley, S., Herraiz-Borreguero, L., van Wijk, E., McMahon, C. R., et al. (2021). Seasonal transformation and spatial variability of water masses within MacKenzie polynya, Prydz Bay. *J. Geophys. Res. Oceans* 126, e221JC017748. doi: 10.1029/2021JC017748

Ratnarajah, L., Nicol, S., and Bowie, A. R. (2018). Pelagic iron recycling in the Southern Ocean: Exploring the contribution of marine animals. *Front. Mar. Sci.* 29. doi: 10.3389/fmars.2018.00109

R Core Team (2021). "R: A language and environment for statistical computing version," in *R Foundation for Statistical Computing* (Vienna, Austria). Available at: https://www/R-project.org/.

Rees, C., Pender, L., Sherrin, K., Schwanger, C., Hughes, P., Tibben, S., et al. (2019). Methods for reproducible shipboard SFA nutrient measurement using RMNS and automated data processing. *Limnol. Oceanogr. Methods* 17, 25–41. doi: 10.1002/lom3.10294

Roca-Martí, M., Puigcorbé, V., Iversen, M. H., van der Loeff, M. R., Klaas, C., Cheah, W., et al. (2017). High particulate organic carbon export during the decline of a vast diatom bloom in the Atlantic sector of the Southern Ocean. *Deep Sea Res. II* 138, 102–115. doi: 10.1016/j.dsr2.2015.12.007

Sathyendranath, S., Brewin, R. J. W., Brockmann, C., Brotas, V., Calton, B., Chuprin, A., et al. (2019). An ocean-colour time series for use in climate studies: the experience of the ocean-colour climate change initiative (OC-CCI). *Sensors* 19, 4285. doi: 10.3390/s19194285

Schallenberg, C., Bestley, S., Klocker, A., Trull, T. W., Davies, D., Gault-Ringold, M., et al. (2018). Sustained upwelling of subsurface iron supplies seasonally persistent phytoplankton blooms around the southern Kerguelen plateau, Southern Ocean. *J. Geophys. Res. Oceans* 123, 5986–6003. doi: 10.1029/2018JC013932

Schofield, O., Saba, G., Coleman, K., Carvahlo, F., Couto, N., Ducklow, H., et al. (2017). Decadal variability in coastal phytoplankton community composition in a changing West Antarctic Peninsula. *Deep-Sea Res. I* 124, 42–54. doi: 10.1016/j.dsr.2017.04.014

Smetacek, V. S. (1985). Role of sinking in diatom life-history cycles: ecological, evolutionary and geological significance. *Mar. Biol.* 84, 239–251. doi: 10.1007/BF00392493

Smetacek, V., Assmy, P., and Henjes, J. (2004). The role of grazing in structuring Southern Ocean pelagic ecosystems and biogeochemical cycles. *Ant. Sci.* 16, 541–558. doi: 10.1017/S0954102004002317

Smith, W. O., Ainley, D. G., Arrigo, K. R., and Dinniman, M. S. (2014). The oceanography and ecology of the Ross Sea. *Annu. Rev. Mar. Sci.* 6, 469–487. doi: 10.1146/annurev-marine-010213-135114

Smith, W. O., Asper, V. L., Tozzi, S., Liu, X., and Stammerjohn, S. E. (2011). Surface layer variability in the Ross Sea, Antarctica as assessed by in *situ* fluorescence measurements. *Prog. Oceanogr.* 88, 28–45. doi: 10.1016/j.pocean.2010.08.002

Smith, W. O., Marra, J., Hiscock, M. R., and Barber, R. T. (2000). The seasonal cycle of phytoplankton biomass and primary productivity in the Ross Sea, Antarctica. *Deep-Sea Res. II* 47, 3119–3140. doi: 10.1016/S0967-0645(00)00061-8

Smith, A., Ratnarajah, L., Holmes, T., Wuttig, K., Townsend, A., Westwood, K., et al. (2021). Circumpolar Deep Water and shelf sediments support late summer microbial iron remineralisation. *Global Biogeochem. Cycles* 35, e2020GB00692. doi: 10.1029/2020GB006921

Smith, N., and Trégure, P. (1994). *Physical and chemical oceanography in the vicinity of Prydz Bay, Antarctica* (Cambridge: Cambridge University Press), 25–43.

Spreen, G., Kaleschke, L., and Heygster, G. (2008). Sea ice remote sensing using AMSR-E 89-GHz channels. *J. Geophys. Res. Oceans.* 113, C02S03. doi: 10.1029/2005JC003384

Strutton, P. G., Griffiths, F. B., Waters, R. L., Wright, S. W., and Bindoff, N. L. (2000). Primary productivity off the coast of East Antarctica (80-150°E): January to March 1996. *Deep-Sea Res. II* 47, 2327–2362. doi: 10.1016/S0967-0645(00)00028-X

Strzepek, R. F., and Harrison, P. J. (2004). Photosynthetic architecture differs in coastal and oceanic diatoms. *Nature* 431, 689–692. doi: 10.1038/nature02954

Sumner, M. (2023). "Raadtools: tools for synoptic environmental spatial data," in *R package version 0.6.0.9032*.

Sunda, W. G., and Huntsman, S. A. (1997). Interrelated influence of light, iron and cell size on marine phytoplankton growth. *Nature* 390, 389–392. doi: 10.1038/37093

Takahashi, K. D., Makabe, R., Takao, S., Kashiwasi, H., and Moteki, M. (2022). Phytoplankton and ice-algal communities in the seasonal ice zone during January (Southern Ocean, Indian sector). *J. Oceanogr.* 78, 409–424. doi: 10.1007/s10872-022-00649-2

Takao, S., Hirawake, T., Hashida, G., Sasaki, H., Hattori, H., and Suzuki, K. (2014). Phytoplankton community composition and photosynthetic physiology in the Australian sector of the Southern Ocean during the austral summer of 2010/2011. *Polar Biol.* 37, 1563–1578. doi: 10.1007/s00300-014-1542-6

Takeda, S. (1998). Influence of iron availability on nutrient consumption ratio of diatoms in oceanic waters. *Nature* 393, 774–777. doi: 10.1038/31674

Thomas, P. G., and Green, K. (1988). Distribution of *Euphausia crystallorophias* within Prydz Bay and its importance to the inshore marine ecosystem. *Polar Biol.* 8, 327–331. doi: 10.1007/BF00442023

Trebilco, R., Melbourne-Thomas, J., and Constable, A. J. (2020). The policy relevance of Southern Ocean food web structure: Implications of food web change for fisheries, conservation and carbon sequestration. *Mar. Policy* 115, 103832. doi: 10.1016/j.marpol.2020.103832

van Leeuwe, M. A., and Stefels, J. (2007). "Photosynthetic responses in *Phaeocystis Antarctica* towards varying light and iron conditions," in Phaeocystis, *major link in the biogeochemical cycling of climate-relevant elements*. Eds. M. A. van Leeuwe, J. Stefels, S. Belviso, C. Lancelot, P. G. Verity and W. W. C. Gieskes (Springer, Dordrecht). doi: 10.1007/978-1-4020-6214-8_6

van Leeuwe, M. A., Webb, A. L., Venables, H. J., Visser, R. J. W., Meredith, M. P., Elzenga, J. T. M., et al. (2020). Annual patterns in phytoplankton phenology in Antarctic coastal waters explained by environmental drivers. *Limnol. Oceanogr.* 65, 1651–1668. doi: 10.1002/lno.11477

Vaz, R. A. N., and Lennon, G. W. (1996). Physical oceanography of the Prydz Bay region of Antarctic waters. *Deep-Sea Res. I.* 43, 603–641. doi: 10.1016/0967-0637(96)00028-3

Venkataramana, V., Anilkumar, N., Naik, R. K., Mishra, R. K., and Sabu, P. (2019). Temperature and phytoplankton size class biomass drives the zooplankton food web

dynamics in the Indian Ocean sector of the Southern Ocean. *Polar Biol.* 42, 823–829. doi: 10.1007/s00300-019-02472-w

Vives, C. R., Schallenberg, C., Strutton, P. G., and Westwood, K. J. (2022). Iron and light co-limitation of phytoplankton growth off East Antarctica. *J. Mar. Syst.* 234. doi: 10.1016/j.jmarsys.2022.103774

Waters, R. L., van den Enden, R., and Marchant, H. J. (2000). Summer microbial ecology off East Antarctica (80-150°E): Protistan community structure and bacterial abundance. *Deep Sea Res. II Top. Stud. Oceanogr.* 47, 2401–2435. doi: 10.1016/S0967-0645(00)00030-8

Westwood, K. J., Griffiths, F. B., Meiners, K. M., and Williams, G. D. (2010). Primary productivity off the Antarctic coast from 30°-80°E; BROKE-West survey 2006. *Deep-Sea Res. II.* 57, 794–814. doi: 10.1016/j.dsr2.2008.08.020

Westwood, K. J., Thomson, P. G., van den Enden, R., Maher, L., Wright, S. W., and Davidson, A. T. (2018). Ocean acidification impacts primary and bacterial production in Antarctic coastal waters during austral summer. *J. Exp. Mar. Biol. Ecol.* 498, 46–60. doi: 10.1016/j.jembe.2017.11.003

Williams, G. D., Herraiz-Borreguero, L., Roquet, F., Tamura, T., Oshima, K. I., Fukamachi, Y., et al. (2016). The suppression of Antarctic bottom water formation by melting ice shelves in Prydz Bay. *Nat. Commun.* 7, 12577. doi: 10.1038/ncomms12577

Williams, G. D., Nicol, S., Aoki, S., Meijers, A. J. S., Bindoff, N. L., Iijima, Y., et al. (2010). Surface oceanography of BROKE-West, along the Antarctic margin of the south-west Indian Ocean (30-80°E). *Deep-Sea Res. II.* 57, 738–757. doi: 10.1016/j.dsr2.2009.04.020

Wolf, C., Iversen, M., Klaas, C., and Metfies, K. (2016). Limited sinking of *Phaeocystis* during a 12-day sediment trap study. *Mol. Ecol.* 25, 3428–3435. doi: 10.1111/mec.13697

Wood, S. (2017). *"Generalized Additive Models: An Introduction with R". 2nd edition* (Chapman and Hall/CRC).

Wright, S. W., Thomas, D. P., Marchant, H. J., Higgins, H. W., Mackey, M. D., and Mackey, D. J. (1996). Analysis of phytoplankton of the Australian sector of the Southern Ocean: Comparisons of microscopy and size frequency data with interpretations of pigment HPLC data using the CHEMTAX matrix factorisation program. *Mar. Ecol. Prog. Ser.* 144, 285–298. doi: 10.3354/meps144285

Wright, S. W., and van den Enden, R. L. (2000). Phytoplankton community structure and stocks in the East Antarctic marginal ice zone (BROKE survey, January-March 1996) determined by CHEMTAX analysis of HPLC pigment signatures. *Deep-Sea Res. II.* 47, 2363–2400. doi: 10.1016/S0967-0645(00)00029-1

Wright, S. W., van den Enden, R. L., Pearce, I., Davidson, A. T., Scott, F. J., and Westwood, K. J. (2010). Phytoplankton community structure and stocks in the Southern Ocean (30-80°E) determined by CHEMTAX analysis of HPLC pigment signatures. *Deep-Sea Res. Pt. II.* 57, 758–778. doi: 10.1016/j.dsr2.2009.06.015

Xu, S., Park, K., Wang, Y., Chen, L., Qi, D., and Li, B. (2019). Variations in the summer oceanic pCO_2 and carbon sink in Prydz Bay using the self-organising map analysis approach. *Biogeosciences* 16, 797–810. doi: 10.5194/bg-16-797-2019

Yang, G., Li, C., Sun, S., Zhang, C., and He, Q. (2013). Feeding of dominant zooplankton in Prydz Bay, Antarctica, during austral spring/summer: food availability and species responses. *Polar Biol.* 36, 1701–1707. doi: 10.1007/s00300-013-1387-4

Zapata, M., Rodriguez, F., and Garrido, J. L. (2000). Separation of chlorophylls and carotenoids from marine phytoplankton: a new HPLC method using a reversed phase C-8 column and pyridine-containing mobile phases. *Mar. Ecol. Prog. Ser.* 195, 29–45. doi: 10.3354/meps195029